DESIGNING A PRECIPITATION COLLECTION NETWORK FOR THE ANALYSIS OF STABLE ISOTOPES IN PRECIPITATION IN FLAGSTAFF, ARIZONA

By Emily E. Henderson

A Thesis

Submitted in Partial Fulfillment

of the Requirements for the Degree of

Master of Science

in Environmental Engineering

Northern Arizona University

May 2023

Approved:

Paul Gremillion, Ph.D., PE, Chair

Salli Dymond, Ph.D.

Mark Lamer, MS, PE

ABSTRACT

DESIGNING A PRECIPITATION COLLECTION NETWORK FOR THE ANALYSIS OF STABLE ISOTOPES IN FLAGSTAFF, ARIZONA

EMILY E. HENDERSON

A precipitation collection network was established in the Flagstaff area for the analysis of stable isotope delta values ($\delta^{18}O$ and $\delta^{2}H$). Isotopic data from event-scale sampling during the monsoon and autumn seasons of 2022 are presented. Significant seasonal trends in isotopic composition were observed that correspond to ambient temperatures and atmospheric circulation features. Furthermore, weather radar was used to assist in interpretation of the event-based data by revealing differences in storm pathways and precipitation intensity, thus enabling analysis of spatial and temporal variations in the isotopic composition of samples from multiple individual events. As such, the high-frequency sampling conducted in this study was proven to be a valuable tool for investigating short-term isotopic variability that is commonly masked by seasonal averages. Beginning in the spring of 2023, this network will not only include stations maintained by project personnel but will incorporate additional collection stations supported by citizen-science. By engaging the public in precipitation sampling, the project aims at cultivating a growing record of isotopic data that can be used to provide enhanced insight into local hydrological processes. Furthermore, data quality among precipitation samples is preserved through the deployment of precipitation collectors that have been designed to limit evaporation from samples. Most importantly, the research presented here has established a baseline dataset for the continued collection of stable isotope data in Flagstaff and will facilitate future isotope studies that may be meaningful to local water resource planning and management.

Table of Contents

Table of Figures

Table of Tables

Table of Equations

List of Abbreviations

ENSO	El Niño-Southern Oscillation
GMWL	Global Meteoric Water Line
GNIP	Global Network of Isotopes in Precipitation
LMWL	Local Meteoric Water Line
NAM	North American Monsoon
NOAA	National Oceanic and Atmospheric Administration
PDO	Pacific Decadal Oscillation

1 Introduction

The city of Flagstaff is located on a plateau within Northern Arizona's Coconino County and sits at an elevation of approximately 6,900 feet. Flagstaff is positioned at the base of Arizona's tallest peak (12,637 feet) and is surrounded by the country's largest ponderosa pine forest. Due to its location within the southwestern United States, Flagstaff is subject to highly variable monsoonal storm events from mid-June through September [1]. At the same time, the combination of Flagstaff's densely forested landscape with hot and arid conditions during the summer months creates the perfect setting for wildfires to arise. The intersection of these characteristics often negatively impacts the people of Flagstaff by increasing the potential for flooding in the region. Furthermore, the unpredictability of these seasonal variables complicates local water resource management. Meanwhile, rising temperatures in the southwestern United States will likely cause Coconino County to experience more frequent and severe drought, more intense storm events, and a growth in the amount of precipitation falling as rain during seasons that historically receive snowfall [2]. Given these circumstances, there is a well-defined need for local hydrological data that can help explain how precipitation from various types of weather systems contributes to water resources in Flagstaff.

Since the 1950s, stable isotope tracers have proven to be a highly effective method for understanding hydrologic processes in watersheds. Unlike internal watershed point measurements, isotope tracers integrate small-scale variability to provide an effective indication of catchment-scale processes [3]. Accordingly, stable isotope data are valuable to water resources investigation, planning, conservation, and development. These data historically represent monthly composite samples, as required by datasets included in the Global Network of

Isotopes in Precipitation (GNIP) [4], but event-scale analysis can also be used to evaluate short-term isotopic variability. Some applications of stable isotope delta values ($\delta^{18}O$ and $\delta^{2}H$) in precipitation include the identification of primary groundwater recharge seasons and source elevations, quantification of soil infiltration rates, and estimation of contributions to streamflow. In Flagstaff, for example, the isotopic content of precipitation and streamflow can be co-analyzed to assess stormwater flowpaths and predict sources of runoff generation. The information gained from that analysis can then be used to improve flood control projects in Coconino County. Currently, limited data is available regarding stable isotope ratios in precipitation in Northern Arizona.

The most recent study regarding stable isotopes in precipitation in Northern Arizona, by Beisner et al. [5], investigated the effects of elevation on stable isotope ratios. In their work, bi-annual precipitation samples from ten stations spread across the Verde River watershed of north-central Arizona were analyzed for $\delta^{18}O$ and $\delta^{2}H$ between 2003 and 2014. Two of those stations were located in Flagstaff, at elevations of 7,100 and 8,100 feet. The data from this research was used to update the local meteoric water line (LMWL) equation and winter and summer precipitation elevation gradients originally published by Blasch and Bryson [6] for the Camp Verde-Flagstaff transect. Thereafter, nearly a decade has passed since stable isotope delta values in precipitation have been recorded in Flagstaff. Even more so, temporal and spatial variations of stable isotopes in precipitation are not well-documented in Northern Arizona due to a lack of small frequency precipitation data. Not to mention, climatic conditions in Coconino County likely differ from those reported in past literature regarding this subject due to the influences of climate change. This paper presents $\delta^{18}O$ and $\delta^{2}H$ values from event-scale precipitation

collection in Flagstaff during the monsoon and autumn seasons of 2022 and introduces a method for continued stable isotope data collection in Coconino County.

2 Isotopic Processes

2.1 Principles of Isotopes in Precipitation

The isotopic composition of precipitation varies due to fractionation, the relative partitioning of isotopes based on their mass differences [3]. These mass differences cause the isotopes of an element to have unique physical and chemical properties. In water, the heavier molecules (HDO, $H_2{}^{18}O$) occur preferentially in the more condensed phase, while the lighter molecule ($H_2{}^{16}O$) is distributed in the remaining phase. For example, in water undergoing evaporation, $H_2{}^{16}O$ will more readily vaporize while $H_2{}^{18}O$ remains in the liquid state. Similarly, in water vapor experiencing condensation, $H_2{}^{18}O$ will preferentially condense to form water droplets while $H_2{}^{16}O$ persists in the vapor phase. This fractionation process ultimately results in a "rainout" phenomenon, the progressive raining out of the heavier water molecules in a moisture mass [7]. Water that is high in $\delta^{18}O$ and $\delta^{2}H$ is termed "enriched", whereas water that is low in $\delta^{18}O$ and $\delta^{2}H$ is called "depleted".

The relationship between $\delta^{18}O$ and $\delta^{2}H$ in water, known as deuterium-excess (d-excess), is defined as d-excess = $\delta^{2}H - 8\delta^{18}O$ [8]. In mid- to high-latitude regions, d-excess is strongly correlated to the physical parameters of the vapor source area, including relative humidity, ambient temperature, and sea surface temperature [9]. These environmental conditions influence the isotopic fractionation of water molecules and, therefore, d-excess measurements reflect the slower rate of diffusion of $\delta^{18}O$ relative to $\delta^{2}H$. The faster movement of the $\delta^{2}H$ molecules leads to non-equilibrium conditions if the two phases are not given enough time to reach isotopic

equilibrium [10]. Accordingly, d-excess serves as an index of deviation from the global meteoric water line (GMWL) and can be used to identify moisture source regions, as well as indicate the degree to which an air mass has undergone evaporation during transport [11]. The GMWL represents the co-variance between $\delta^{18}O$ and $\delta^{2}H$ concentrations observed in most meteoric waters around the world [12]. The regression line derived from this co-variance may be explained by the condensation of water vapor under near-equilibrium conditions that evaporated during nonequilibrium conditions [7].

Fractionation processes cause isotopic variations both geographically and temporally due to two major factors: temperature, and the portion of original water vapor remaining in the parcel of air that is experiencing precipitation [7]. These controlling factors have been observed as effects due to continental location, elevation, latitude, and amount of precipitation. Continental location affects the isotopic composition of meteoric waters due to fractionation that occurs as an air mass progresses further inland, away from its source of moisture (the ocean), resulting in increasingly depleted precipitation [7]. Correspondingly, meteoric waters are observed to be progressively more depleted as elevation is gained. The elevation effect is caused by increased rainout at higher elevations due to orographic lifting and is compounded by greater fractionation between liquid and vapor at lower temperatures [7]. Similarly, higher latitudes are also known to receive precipitation that is more isotopically depleted as the result of heightened rainout and increased fractionation induced by colder temperatures [7]. Finally, the amount effect is the observation that larger storm events produce precipitation that is more depleted than minor events. During smaller storm events, precipitation may become more isotopically enriched due to evaporation that occurs as it falls through air of low humidity. These evaporative effects are typically reduced

during longer rainstorms, as they create more saturated conditions in the air beneath the cloud base and, therefore, less enrichment [7].

2.2 Precipitation in Flagstaff

Precipitation in Flagstaff primarily falls during two distinct periods. From November through April, precipitation is produced exclusively by frontal systems that convey atmospheric moisture eastward off the Pacific Ocean [13]. The other period of precipitation, occurring from July through September, is delivered by the North American Monsoon (NAM) [14]. This atmospheric phenomenon develops in mid-June and is characterized by a significant increase in rainfall over the southwestern Unites States and northwestern Mexico. During the NAM, high-intensity convective storms migrate north from the Gulf of California as the result of a seasonal reversal in wind direction that is facilitated by intense solar radiation in the region [15]. Mid-level moisture from the Gulf of Mexico has also been known to partially contribute to monsoon activity. These characteristic atmospheric moisture transport patterns are displayed in Figure 2.1 [1].

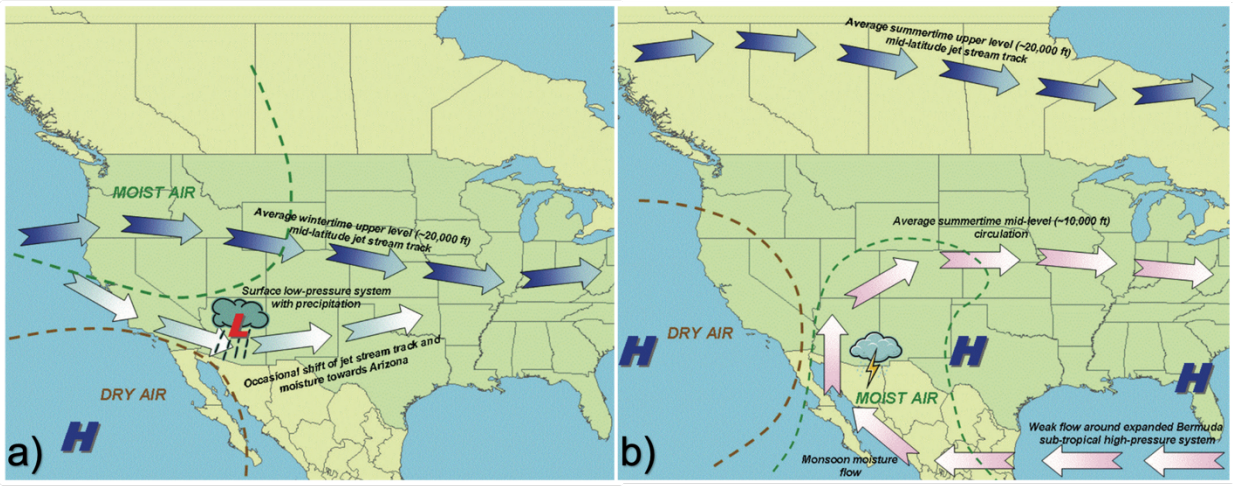

Figure 2.1 Average atmospheric flow patterns and moisture airmass boundaries for (a) autumn and (b) monsoon [1]

Annual precipitation in Flagstaff is highly variable due to the influences of the El Niño-Southern Oscillation (ENSO), Pacific Decadal Oscillation (PDO), and NAM [2]. ENSO is a periodic change (every 2-7 years) in Pacific sea surface temperature that directly impacts precipitation patterns in the United States [16]. Similarly, the PDO is a long-term (every 20-30 years) fluctuation of sea surface temperature in the Pacific Ocean that affects weather in the United States by altering the path of the jet stream [17]. The total annual precipitation received in Flagstaff over the last 30 years is shown in Figure 2.2, using data from the National Oceanic and Atmospheric Administration's (NOAA's) station at the Flagstaff Pulliam Airport [18].

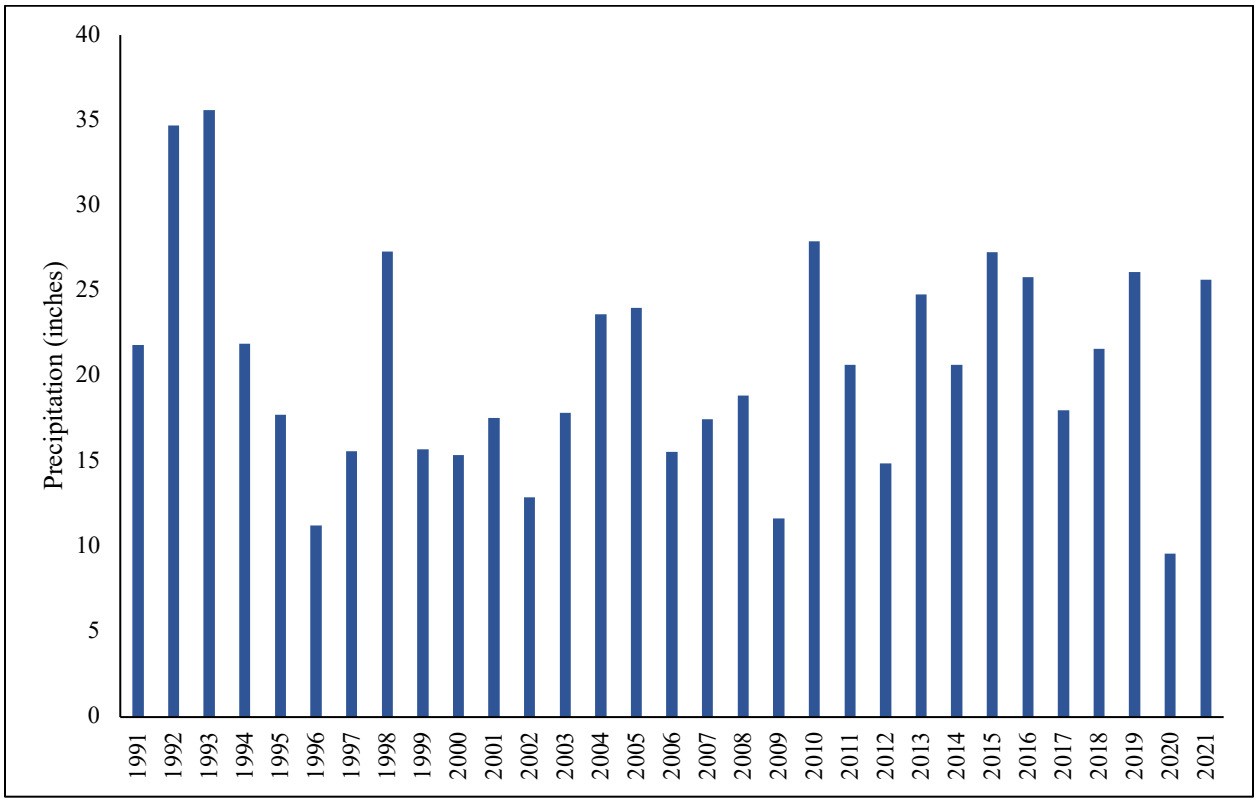

Figure 2.2 Total Annual Precipitation at the Flagstaff Pulliam Airport from 1991-2001

Over the last five years, the NAM seasons contribution to total annual precipitation in Flagstaff ranged from 10-61%. Of which, only two years had NAM seasons that provided less

than 45% of the city's total annual precipitation. The monthly precipitation patterns from 2017 to 2021 are displayed in Figure 2.3 and Figure 2.4 [18]. Figure 2.3 includes all monthly precipitation, while Figure 2.4 only shows snowfall. Although monthly precipitation averages fluctuate from year to year, Flagstaff typically receives the most rainfall during the monsoon months of July and August. Winter weather typically emerges by November as temperatures begin dropping and snowfall appears. Snow usually remains the dominant form of precipitation until mid-April when ambient temperatures begin rising again.

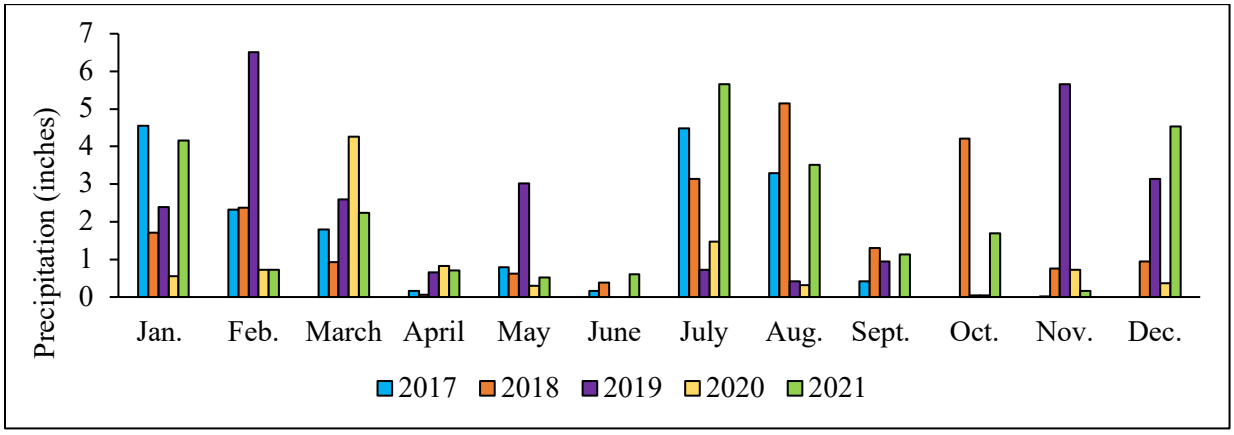

Figure 2.3 Precipitation in Flagstaff from 2017 – 2021

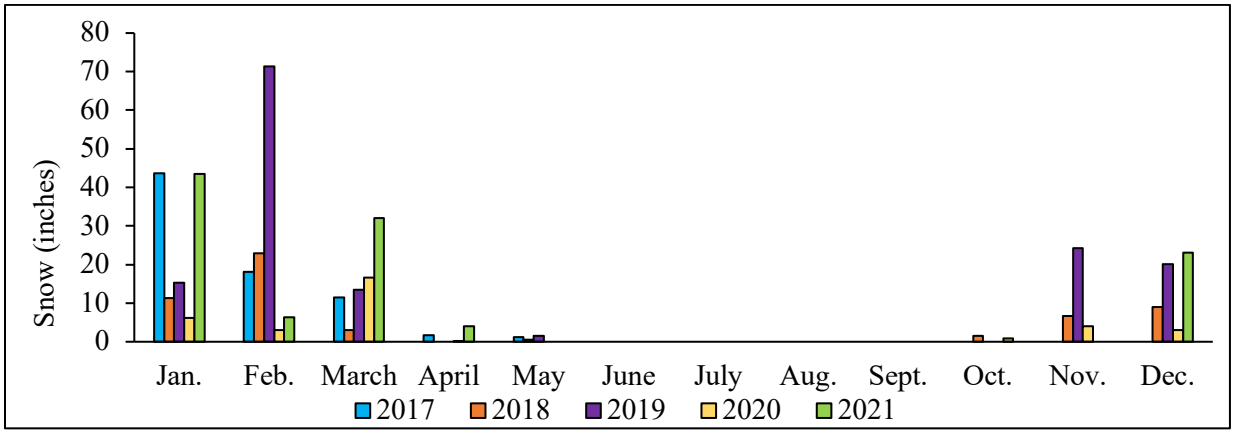

Figure 2.4. Monthly Snowfall in Flagstaff from 2017 – 2021

Over the last 30 years, monsoonal precipitation totals in Arizona have generally declined as compared to the previous climate normals [19]. This effect is the result of climate change, where

warming temperatures have expanded and intensified the NAM ridge, leading to less storm events in Arizona during the peak of the monsoon season [20]. However, during the late monsoon season, areas of Northern Arizona have been observed to experience an increase in total precipitation caused by increased rainout at higher elevations. Although fewer storm events are occurring on average, the most extreme storms are becoming more intense due to the extra moisture-holding capacity of a warmer atmosphere. Furthermore, the storm systems that develop over these mountainous areas are traveling less frequently into the lower deserts, thus heightening potential flooding at the upper elevations [20]. As was previously mentioned, the most recent data on stable isotopes in precipitation in Flagstaff was collected between 2003 and 2014. The Flagstaff station at 7,100 feet in elevation had a summer (April – November) LMWL of $\delta^2H = 7.94\delta^{18}O + 9.58$, with a significant decline in stable isotope delta values over time. The average d-excess for summer precipitation was 10.03‰ [5]. Additionally, Tulley-Cordova et al. [21] conducted a stable isotope study from 2014 to 2017 that analyzed precipitation from the Navajo Nation (a region northeast of Flagstaff that includes portions of Arizona, New Mexico, and Utah) that was associated with the NAM. In their work, the mean monsoon values for $\delta^{18}O$ and δ^2H were -5.7‰ and -41.6‰, respectively.

3 Stable Isotope Delta Values of Precipitation in Flagstaff during Monsoon and Autumn of 2022

From late June to early November, a total of 131 precipitation samples were collected throughout Flagstaff and analyzed for stable isotope delta values. As expected, Flagstaff received the largest amount of rainfall during the monsoon months of July and August. Figure 3.1 shows the amount of daily precipitation experienced at the Flagstaff Airport weather station during the

monsoon and autumn seasons of 2022, as well as the average daily temperature. When compared to the monthly totals from the last 30 years (1991 – 2021), June, July, and August received less than average amounts of precipitation, while above average totals were recorded for September, October, and November.

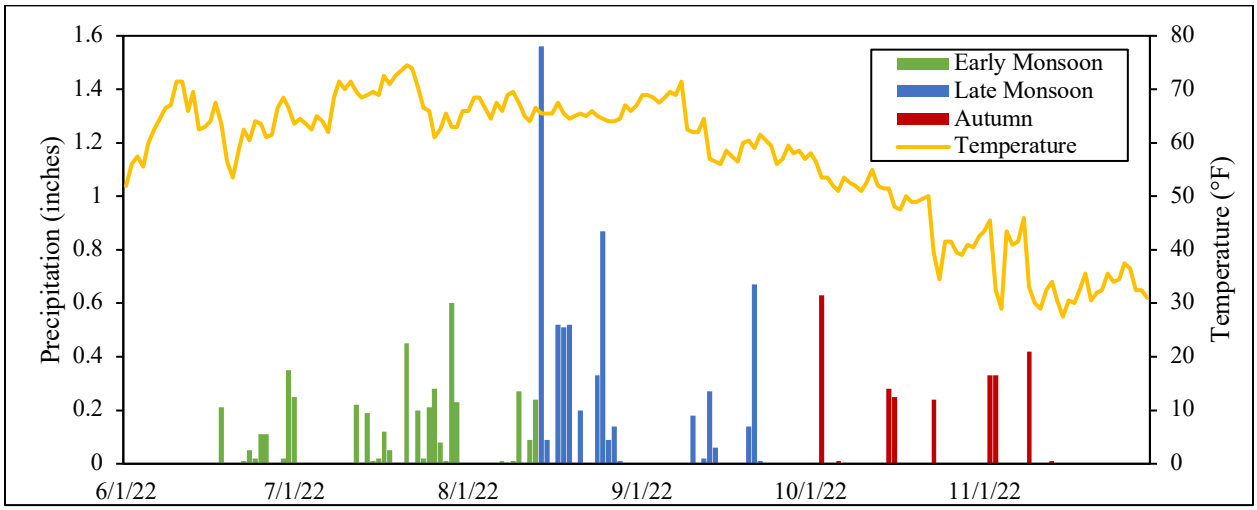

Figure 3.1 Daily precipitation amount in Flagstaff from June to November 2022

3.1 Methodology

This section describes the methods used for sample collection and analysis.

3.1.1 Sample Collection

Monsoon precipitation collection began on June 23, 2022, with the first monsoonal rain of the year. Due to the quick onset of the monsoon season and limited resources, the collectors were built using materials that were cost-effective and easy to acquire. Each collector was comprised of a funnel attached to a 500 mL HDPE-Nalgene bottle and was secured to a free-standing pole, away from the interference of tall buildings and trees. A plastic table-tennis ball was placed at the mouth of the funnel to reduce evaporation from the sample bottle, and samples were typically collected immediately after the storm event. Initially, five stations were established over a 3.5-

mile radius for event-based sampling (Table 3.1, Figure 3.2). The O'Leary station was only in operation during June and July before being taken offline.

Table 3.1 Locations of Precipitation Collectors

Collector ID	Latitude	Longitude	Elevation (ft)
Soliere	35.2119	-111.5797	6,764
O'Leary	35.1902	-111.6469	6,892
Beulah	35.1607	-111.6849	6,924
Windtree	35.1947	-111.6859	7,066
Engineering	35.1767	-111.6572	6,904

Additionally, snow collectors were built for precipitation collection towards the end of the autumn season. These were created using 4-inch diameter PVC pipe and end caps. A design height of 10 inches was chosen using the last five years of snowfall data in Flagstaff, where over 80% of the daily snowfall events resulted in less than 10 inches of accumulated snow. Following collection, the snow collectors were capped for 24 hours to allow for melting. The majority of samples were collected directly after the storm event, with the exception of samples from overnight storms which were collected at sunrise the following morning. Additionally, multiple intra-event samples were collected at the Beulah station on August 14th, 2022. In most cases, the volume of each precipitation sample was recorded after collection to determine the associated precipitation depth. In instances where the volume was not recorded, local rain gauge data from NOAA is used as a substitute. All precipitation samples were transferred from the collection device into 50 mL centrifuge tubes for storage at room temperature prior to analysis. The samples were stored with no headspace when the sample volume was at least 50 mL.

Figure 3.2 shows the locations of the five collection stations. Notice that terrain becomes more mountainous directly to the north of the collection stations, corresponding to the areas of higher elevation surrounding Mount Elden and Mount Humphreys.

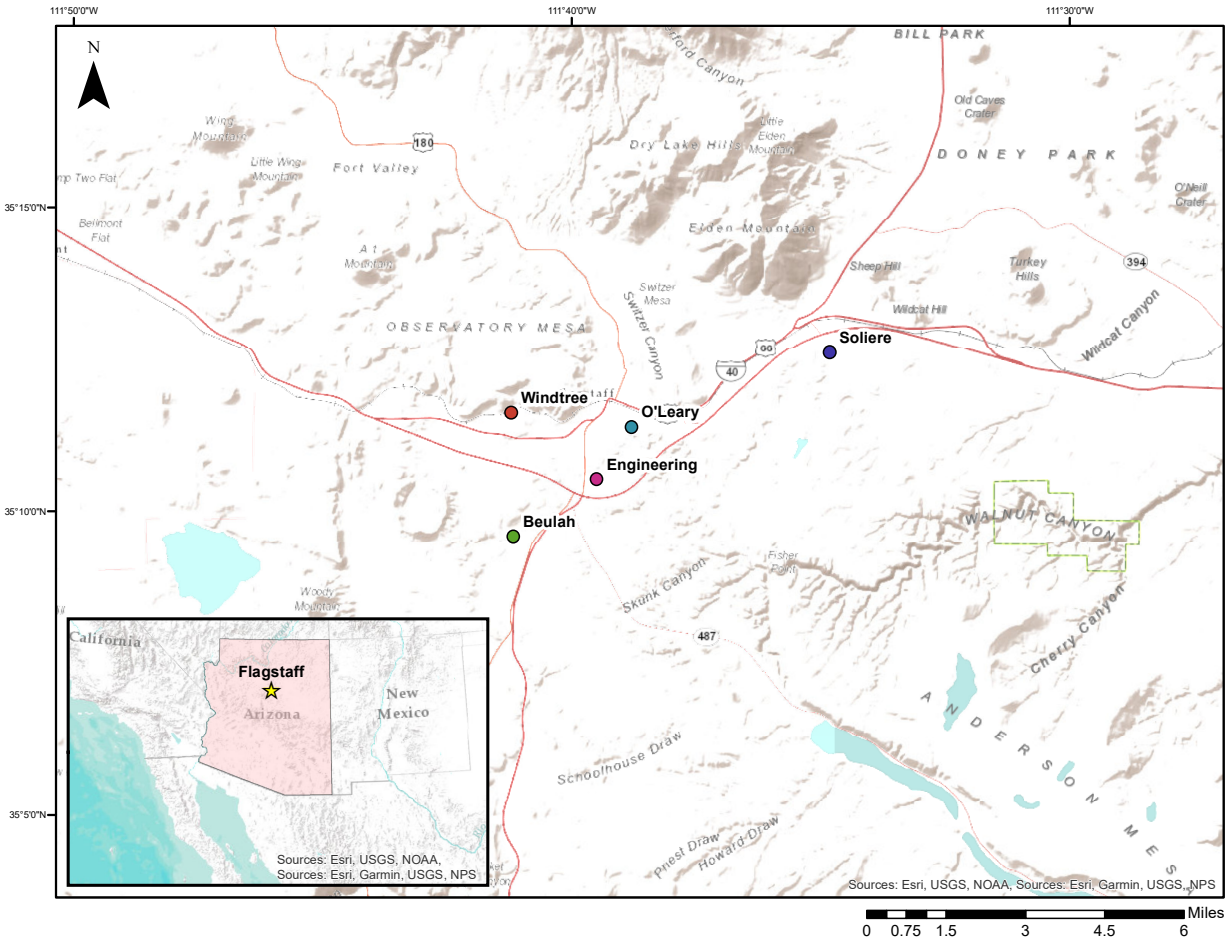

Figure 3.2 Map of precipitation collection stations

3.1.2 Sample Analysis

The precipitation samples were divided into three seasons (early monsoon, late monsoon, and autumn) to assess the temporal variability of stable isotope ratios. Early monsoon includes precipitation from June 23 to July 13, late monsoon includes precipitation from July 14 to September 30, and autumn includes precipitation from October 1 to November 9. All samples were measured for $\delta^{18}O$ and $\delta^{2}H$ with a Picarro Cavity Ring-Down Spectrometer at the Arizona

Climate and Ecosystems Isotope Laboratory at Northern Arizona University. Prior to analysis, each sample was filtered with a 0.2-micron membrane filter. Stable isotope delta values are reported in δ notation, relative to Vienna Standard Mean Ocean Water (VSMOW). All $\delta^{18}O$ and $\delta^{2}H$ data from individual samples are found in Section 9.1: Appendix A.

3.1.3 Statistical Analysis

For a particular event date, the $\delta^{18}O$ and $\delta^{2}H$ values among the samples from all stations were averaged to estimate a singular daily mean (Section 9.2: Appendix B). Furthermore, weekly mean delta values were calculated by averaging the mean daily delta values from a given week. This was done to assess the variability of isotopic content on a weekly basis. For all three seasons, the daily mean stable isotope data follow a normal distribution, as confirmed using the Shapiro-Wilk normality test ($p > 0.05$). Since the data were approximately normally distributed, the empirical rule was employed to identify any outliers within the dataset. That is, an observation was considered an outlier if it was more than three standard deviations away from the mean. Using this rule, no outliers were detected within the dataset.

3.2 Results

The mean daily values for $\delta^{18}O$, $\delta^{2}H$, and deuterium excess (d-excess) over the entire sampling period are presented in Table 3.2.

Table 3.2 Mean daily stable isotope delta values

No. of Obs.	$\delta^{2}H$ (mean ± SD), ‰	$\delta^{18}O$ (mean ± SD), ‰	d-excess (mean ± SD), ‰
53	-32.44 ± 22.30	-5.48 ± 3.16	8.48 ± 6.58

The LMWL (Equation 3.1) was developed from a linear regression analysis ($R^2 = 0.93$) performed on the data and represents the covariation of hydrogen and oxygen stable isotope ratios during the sampling period.

Equation 3.1 Local Meteoric Water Line

$$\delta^2 H = 6.83\delta^{18} O + 3.12$$

Figure 3.3 shows the relationship between $\delta^{18}O$ and δ^2H, as well as the LMWL and GMWL ($\delta^2H = 8\delta^{18}O + 10$). Each season contains a large percentage of samples whose isotope ratios plot near the GMWL, which is a property of most precipitation that has not been impacted by partial evaporation after condensation [8]. Still, the early monsoon and late monsoon periods contain a handful of samples that plot well below the GMWL, indicating that the samples have experienced some degree of evaporation. Since the collection devices were fashioned to limit evaporation from the sample bottle and samples were stored without headspace, it is unlikely that significant evaporative loss occurred after collection. Therefore, it is more probable that the hot and dry summer atmosphere enabled sub-cloud evaporation to occur in some samples, as has been observed to occur in arid climates [7]. All autumn precipitation plotted above or along the GMWL. The seasonal linear trendline slopes are as follows: early monsoon = 6.55 ($R^2 = 0.91$), late monsoon = 7.35 ($R^2 = 0.94$), autumn = 8.17 ($R^2 = 0.97$). The slope of the early monsoon LMWL deviated the most from the GMWL, which is understandable given that the early monsoon featured the warmest average temperatures and most arid conditions.

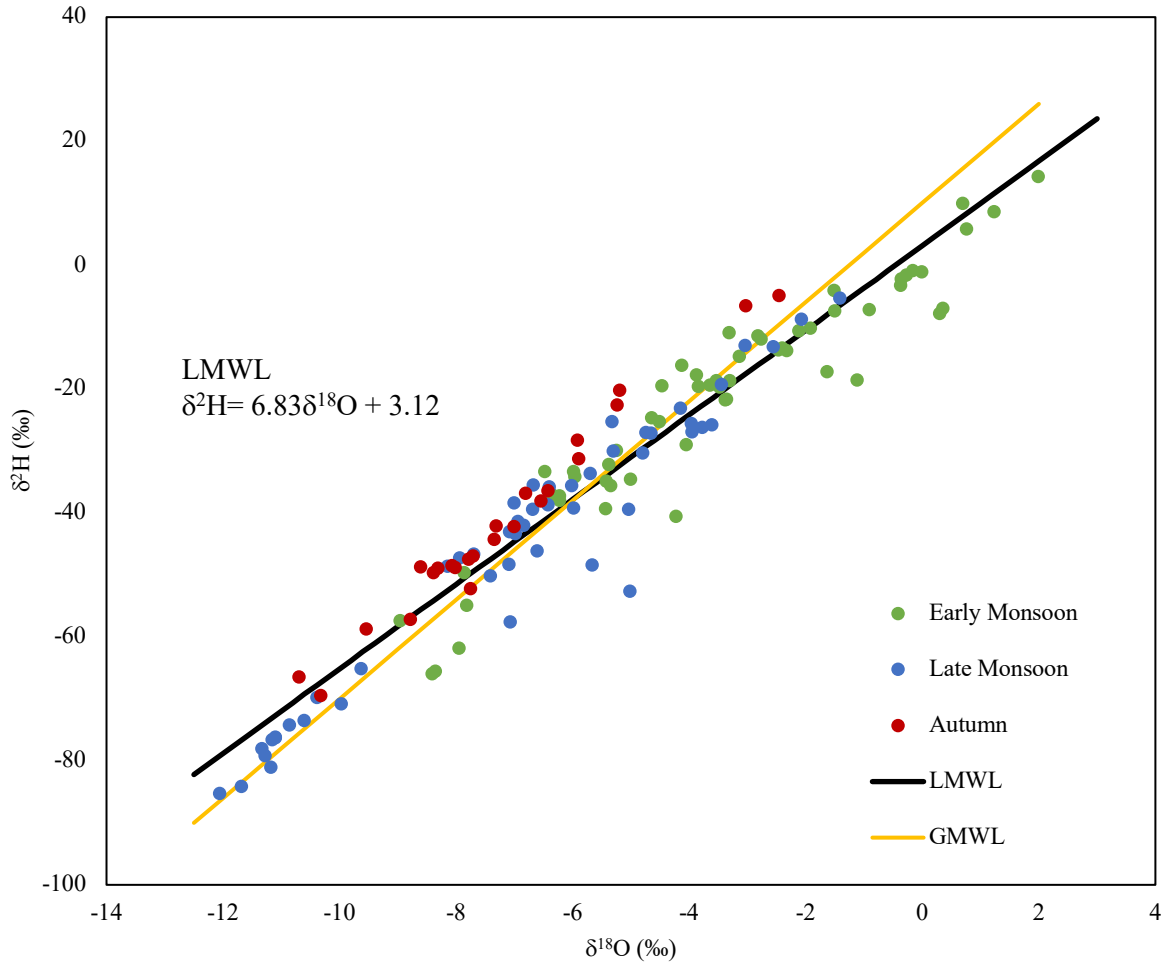

Figure 3.3 Monsoon and autumn δ^2H and $\delta^{18}O$ ratios as compared to the LMWL and GMWL

The seasonal mean and standard deviation (SD) values for $\delta^{18}O$, δ^2H, and d-excess are summarized in Table 3.3.

Table 3.3 Seasonal Summaries of Stable Isotope Values

Season	No. of Obs.	Mean Ambient Temp. (°F)	δ^2H (mean ± SD), ‰	$\delta^{18}O$ (mean ± SD), ‰	d-excess (mean ± SD), ‰
Early Monsoon	28	67	-21.03 ± 19.69	-3.30 ± 2.78	5.29 ± 6.17
Late Monsoon	17	63	-44.28 ± 22.15	-6.80 ± 2.79	9.53 ± 5.05
Autumn	9	46	-41.36 ± 16.16	-7.22 ± 1.90	16.36 ± 2.34

Early monsoon precipitation was generally enriched in both stable isotopes as compared to the latter seasons. During the early monsoon, $\delta^{18}O$ and $\delta^{2}H$ values ranged from -8.97 to 1.98‰ and -65.93 to 14.33‰, respectively. Precipitation during the late monsoon was the most depleted in deuterium and showed the highest variability in $\delta^{18}O$ and $\delta^{2}H$ ratios. Late monsoon $\delta^{18}O$ and $\delta^{2}H$ values varied from -12.07 to -1.42‰ and -85.22 to -5.32‰, respectively. On average, autumn precipitation was the most depleted in $\delta^{18}O$ and exhibited the smallest range in isotopic composition. $\delta^{18}O$ and $\delta^{2}H$ values in autumn ranged between -10.70 to -2.47‰ and -69.36 to -4.87‰, respectively. The seasonal means of $\delta^{18}O$ declined over time, however, the same trend was not observed of $\delta^{2}H$. The data were plotted as probability density functions (Figure 3.4) to better investigate the seasonal distributions of the stable isotope values. The density distributions revealed that the peaks in $\delta^{18}O$ and $\delta^{2}H$ values were in fact more negative as the seasons progressed.

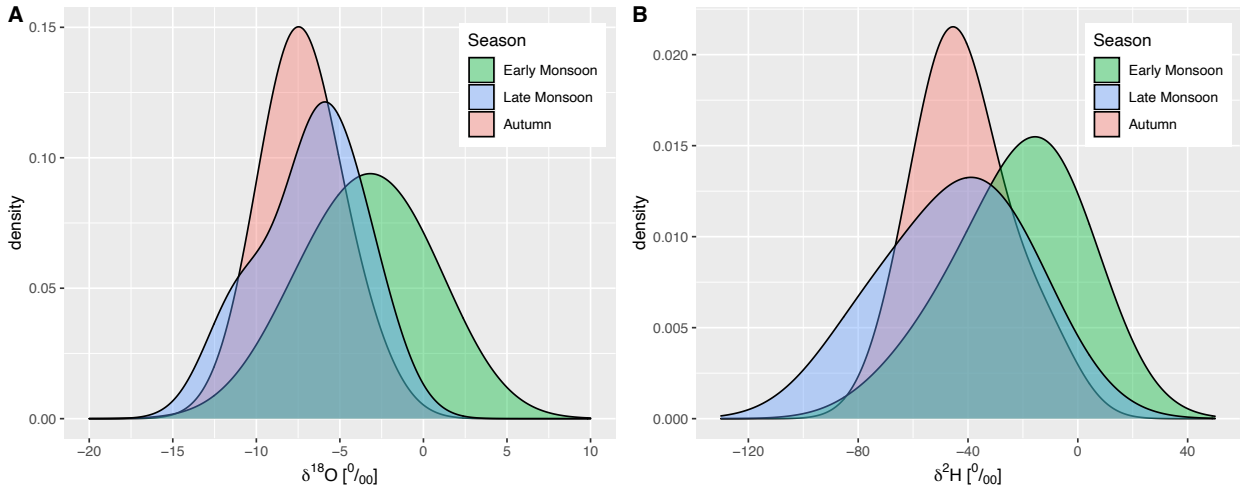

Figure 3.4 (A) distribution of $\delta^{18}O$ values by season; (B) distribution of $\delta^{2}H$ values by season

A more granular view of the temporal fluctuations in $\delta^{18}O$ and $\delta^{2}H$ is presented in Figure 3.5 and Figure 3.6, where $\delta^{18}O$ and $\delta^{2}H$ followed a nearly identical pattern. During the early

monsoon season, stable isotope values generally were increasingly enriched until peaking on June 22nd. Following this peak, stable isotope ratios were progressively depleted over the duration of the late monsoon. The last monsoonal rain was followed by a period of eight dry days before the first precipitation event of autumn arrived. When compared to the last monsoon event, autumn precipitation began with significantly higher delta values that became more depleted over time.

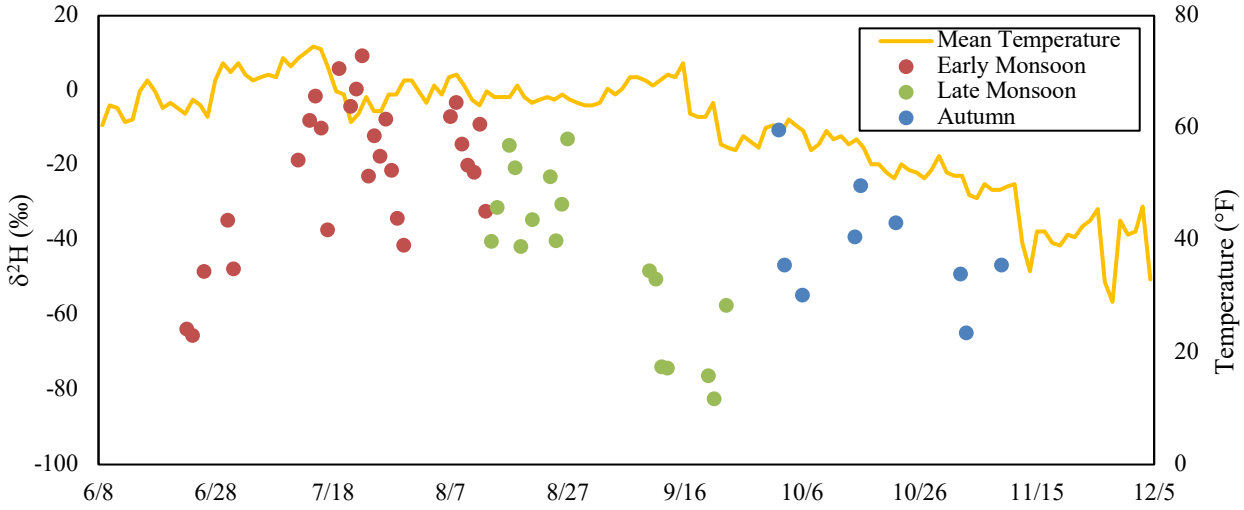

Figure 3.5 Temporal Variability in δ^2H

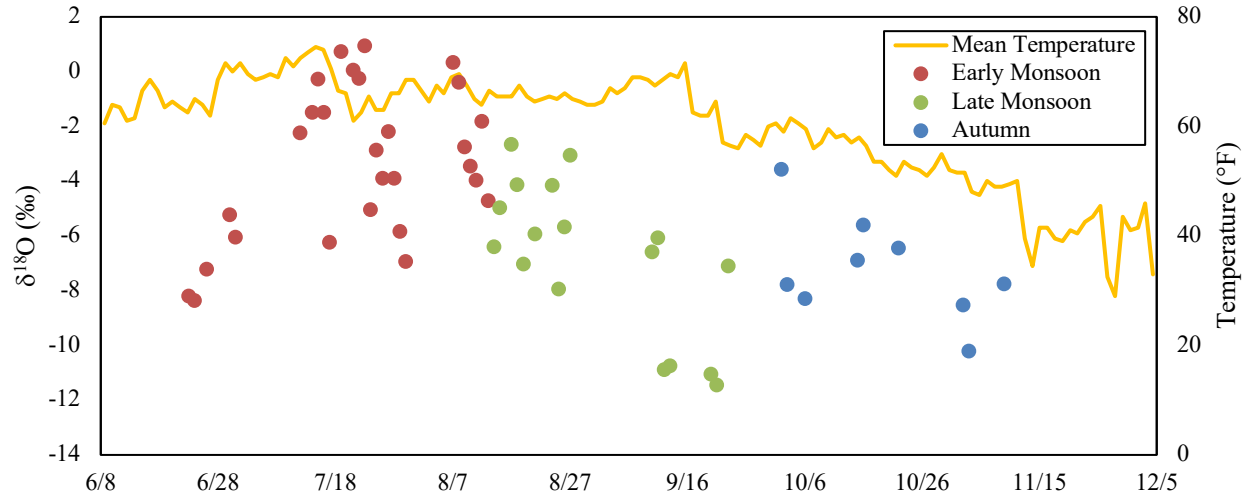

Figure 3.6 Temporal Variability in $\delta^{18}O$

These trends have been further summarized by week in Table 3.4. Of the twenty-one weeks under consideration, five weeks do not contain stable isotope data due to lack of precipitation.

Table 3.4 Weekly Summaries of Stable Isotope Values

Week of (2022)	Precip. Amount (in)	No. of Obs.	Mean Ambient Temp. (°F)	δ^2H (mean ± SD), ‰	$\delta^{18}O$ (mean ± SD),‰	d-excess (mean ± SD),‰
Early Monsoon						
June 19	0.19	2	59.9	-64.68 ± 1.19	-8.27 ± 0.12	1.50 ± 0.23
June 26	0.73	3	64.6	-43.53 ± 7.71	-6.15 ± 1.00	5.32 ± 4.11
July 3	0	0	65.3			
July 10	0.44	4	69.6	-9.53 ± 7.02	-1.36 ± 0.80	1.37 ± 1.96
July 17	0.82	4	72.6	-8.84 ± 19.37	-1.42 ± 3.24	2.49 ± 7.35
July 24	1.43	7	63.9	-22.47 ± 11.88	-4.37 ± 1.67	12.50 ± 2.74
July 31	0	0	66.8			
Aug. 7	0.62	7	66.8	-15.37 ± 10.08	-2.38 ± 1.87	3.50 ± 6.51
Late Monsoon						
Aug. 14	3.2	5	65.6	-29.73 ± 11.94	-5.03 ± 1.76	9.92 ± 2.97
Aug. 21	1.63	5	64.9	-28.23 ± 10.57	-5.34 ± 1.86	13.03 ± 2.39
Aug. 28	0	0	67.3			
Sept. 4	0.18	1	67.2	-48.15	-6.57	4.41
Sept. 11	0.35	3	58.9	-66.18 ± 13.67	-9.22 ± 2.74	7.58 ± 8.24
Sept. 18	0.82	3	59.6	-72.11 ± 13.00	-9.85 ± 2.41	6.73 ± 6.75
Sept. 25	0.02	0	57.7			
Autumn						
Oct. 2	0.64	3	53.2	-37.27 ± 23.52	-6.54 ± 2.59	15.03 ± 3.24
Oct. 9	0.28	1	52.2	-39.19	-6.87	15.77
Oct. 16	0.49	2	49.0	-30.37 ± 7.03	-6.01 ± 0.59	17.69 ± 2.30
Oct. 23	0	0	39.5			
Oct. 30	0.66	2	39.6	-56.94 ± 11.13	-9.35 ± 1.19	17.87 ± 1.60
Nov. 6	0.42	1	36.1	-46.64	-7.74	15.29

The first four weeks of the early monsoon season were characterized by a gradual rise in weekly average $\delta^{18}O$ values, simultaneously corresponding to rising ambient temperatures. Stable isotope delta values declined the following week, once again corresponding to a change in

mean ambient temperature. Weekly mean $\delta^{18}O$ became more negative from August 7th through August 21st, while d-excess exhibited the opposite trend. During these three weeks, changes in both d-excess and $\delta^{18}O$ were again correlated with temperature. A similar trend of isotopic depletion with time was observed during the weeks of September 4th through September 18th. The distribution of $\delta^{18}O$ and $\delta^{2}H$ by week is illustrated in Figure 3.7, revealing considerable differences in the isotopic composition of precipitation captured within a relatively short timeframe.

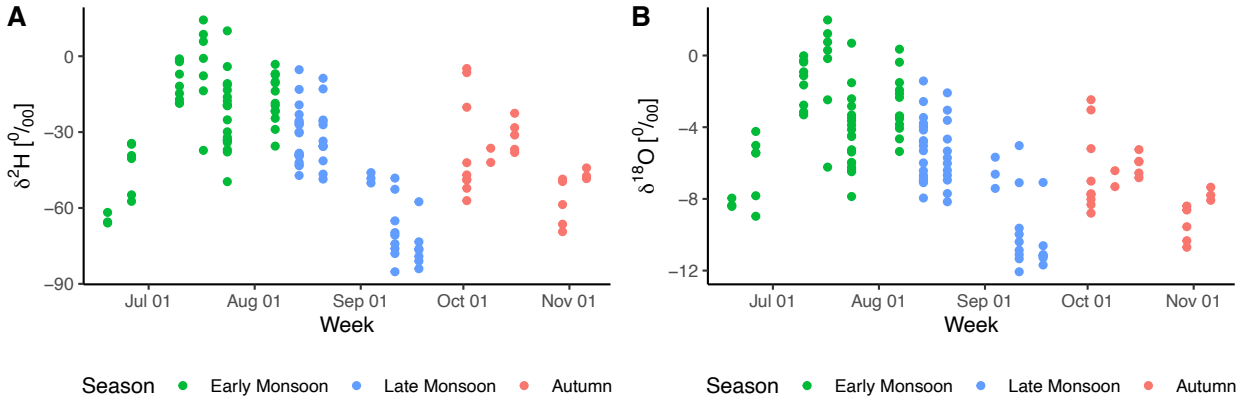

Figure 3.7 Weekly distributions of (A) $\delta^{2}H$ values and (B) $\delta^{18}O$ values in precipitation samples

Following the first dry week of the monsoon season, precipitation was significantly more enriched in both isotopes as compared to the first two weeks. The same pattern of enrichment, to a lesser degree, was also observed after the second dry period occurred three weeks later and following the last week in the late monsoon. Conversely, precipitation samples were also observed to be more isotopically depleted after the third and fifth dry weeks when compared to earlier weeks. Although stable isotope ratios fluctuated over the course of the sampling period, d-excess exhibited strong correlations with respect to both time ($r = 0.80$) and temperature ($r = -0.78$). These relationships are displayed in Figure 3.8, along with their respective linear

regression trendlines. The grey shading in each plot represents the 95% confidence interval of the linear regression analysis.

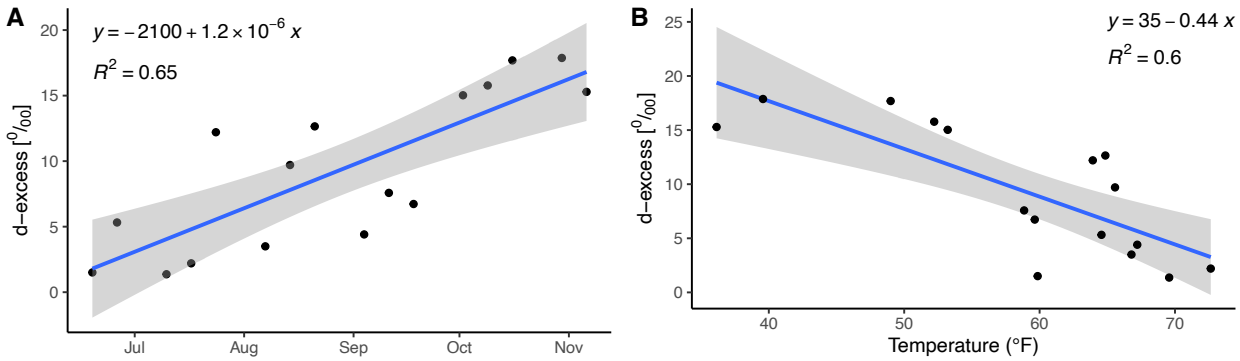

Figure 3.8 Relationship between weekly mean d-excess and (A) time and (B) temperature

3.2.1 Variations in stable isotope delta values on small spatial and temporal scales

Large variations in the isotopic composition of precipitation have previously been observed from storm systems on small geographic and temporal scales [7]. For instance, the measured $\delta^{18}O$ and $\delta^{2}H$ in precipitation samples from a distinct convective storm in southern Nevada differed by 1.5 and 15%, respectively, for a range of less than 3 kilometers (1.9 miles) [22]. Likewise, sequential precipitation samples collected from one station during a single storm in the Sierra Nevada mountain range exhibited deuterium differences of up to 114% [23]. To examine the spatial and temporal isotopic trends occurring within the Flagstaff dataset, samples were subdivided into the following multi-day groupings: June 23rd – July 1st, July 12th – 17th, July 20th – 30th, August 7th – 19th, August 21st – 27th, September 10th – 23rd, October 2nd – 6th, October 15th – 22nd, November 2nd – 9th. Among the five sampling stations, there is no statistically significant difference in either the mean d-excess or mean stable isotope delta values of daily samples (ANOVA, p-value > 0.05). The distribution of $\delta^{18}O$ and $\delta^{2}H$ measurements by

station is illustrated in Figure 3.9. All the stations present similar distributions in their sample data, apart from the O'Leary station that only collected early monsoon data.

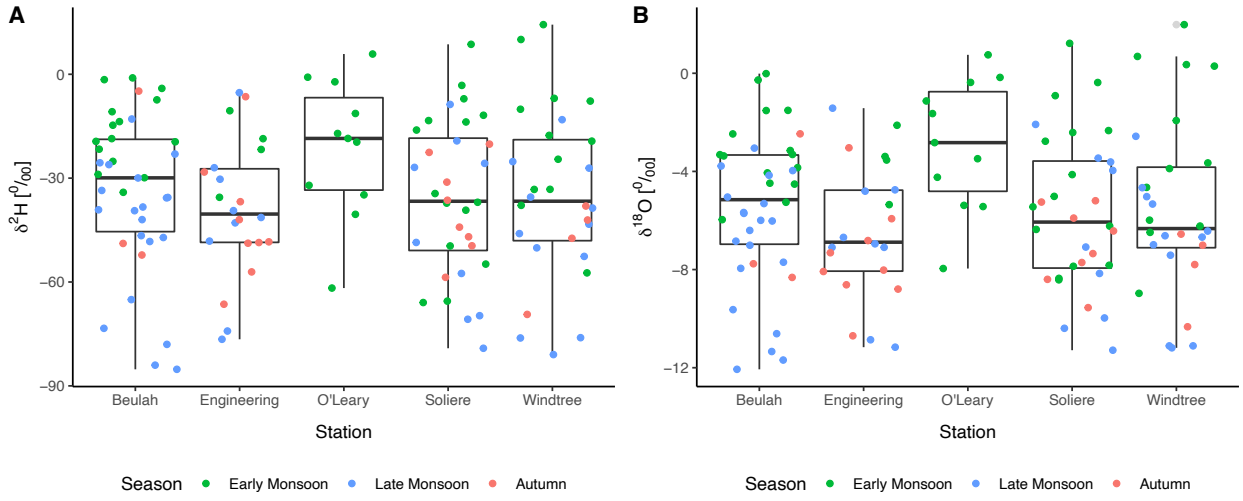

Figure 3.9 Distribution of (A) δ^2H values and (B) $\delta^{18}O$ values by station

Weather radar data from NOAA's Climate and Weather Toolkit [24] was used to evaluate the relationship between an air mass's trajectory, precipitation duration and intensity, and the corresponding spatial distribution of stable isotope delta values. All observations related to storm trajectory and precipitation intensity are inferred from weather radar time series data. Early monsoon precipitation in Flagstaff kicked off with low intensity storm systems migrating from the southwest, however, most of the early monsoon and beginning of the late monsoon was dominated by systems originating from the southeast. Winds began to shift from westerly to easterly towards the end of August, prompting air masses to drift into Flagstaff from the west. By autumn, the majority of moisture transport into the area was flowing from the northwest. Additionally, periods of precipitation that were not related to monsoonal storm fronts were identified using weather radar. The following subsections contain the analysis for each of the multi-day groupings.

3.2.1.1 June 23rd to July 1st

Figure 3.10 shows the progression of $\delta^{18}O$ and $\delta^{2}H$ values from the first monsoon rain (June 23rd) to July 1st. During the first two days of this time frame, Flagstaff experienced light to moderate rains that progressed from west to east. On June 23rd, the sample collected from the Soliere station ($\delta^{18}O$ = -8.42‰) was slightly more depleted than the O'Leary sample ($\delta^{18}O$ = -7.96‰) from the same day. Since the O'Leary station is located further west than the Soliere station, this isotopic difference may be attributed to raining out of the heavier isotopes as the air mass traveled further inland. Furthermore, when comparing the two stations, sub-cloud evaporative forces may have been more significant at the O'Leary station since it experienced less intense and less frequent rainfall. In other words, it is probable that the atmosphere around the Soliere collector maintained a higher degree of saturation, thus reducing the likelihood of evaporative enrichment during the precipitation's descent.

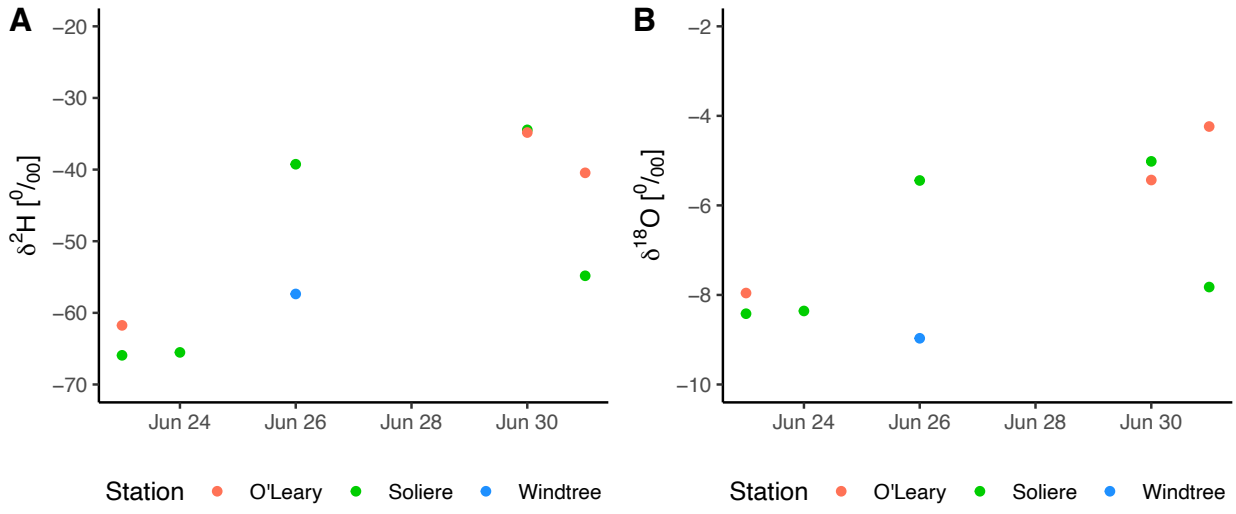

Figure 3.10 Variation in (A)$\delta^{2}H$ and (B) $\delta^{18}O$ from June 23rd to July 1st

Between June 24th and June 26th, weather radar indicated that atmospheric moisture was not carried into Flagstaff, but rather developed from local evapotranspiration. Correspondingly,

samples collected on June 26th were more enriched in deuterium than samples from the prior days. Still, a significant difference was seen between the isotopic composition of the two samples collected that day. This variation is most likely due to differences between the trajectories of the air masses. Unlike the storm systems that traveled inland from the southwest, the saturated air masses produced from local evapotranspiration did not migrate in one uniform direction, but instead developed around multiple areas in Flagstaff and traveled in an unpredictable manner. In this case, precipitation began at the Soliere collector before moving north towards Mount Elden, where rainfall intensified at the higher elevations. This air mass continued to rainout at the higher elevations while progressing eastward towards the Windtree collector. Therefore, the disparity between the isotopic ratios in the Soliere and Windtree samples may be the result of a rainout effect occurring between the collectors, facilitated by the air mass's flow path over an area of higher elevation.

The June 26th event was followed by a period of three precipitation-free days before a convective system migrating from the southwest arrived in Flagstaff on June 30th. Once again, this precipitation was more isotopically enriched compared to the most recent storm event. During this short dry period, daily average temperatures in Flagstaff also rose by 7°F. Considering these conditions, it is theorized that the opposite of the continental effect occurred as the air mass progressed further inland. This is to say that the air mass was likely subject to evaporative enrichment as it migrated over the arid landscape of the southwest, thus reversing isotopic depletion of the parent condensing vapor through the return of water to the cloud by evaporation. The precipitation from July 1st was a continuation of the June 30th storm front and, as expected, was more depleted than precipitation captured from the previous day. The rainout effect was observed once again as the sample collected at Soliere ($\delta^{18}O$ = -7.82‰) was more

isotopically depleted than at O'Leary ($\delta^{18}O$ = -4.24‰), coinciding with its location relative to the air mass's trajectory. The raining out of heavier isotopes over the storm's progression eastward resulted in more depleted precipitation at Soliere.

3.2.1.2 July 12th to July 17th

Eleven days passed before the next precipitation event occurred in Flagstaff on July 12th, allowing the daily average temperature in the area to climb by 7°F. Likewise, weather radar indicated that atmospheric moisture on July 12th grew from local evapotranspiration that was facilitated by increasing temperatures. This dry period was succeeded by multiple days of rainfall. Figure 3.11 displays the fluctuations in $\delta^{18}O$ and $\delta^{2}H$ ratios measured in precipitation from July 12th to July 17th. Compared to the most recent precipitation samples collected on July 1st (mean $\delta^{18}O$ = -6.03‰), July 12th precipitation was considerably more enriched in both isotopes (mean $\delta^{18}O$ = -2.22‰).

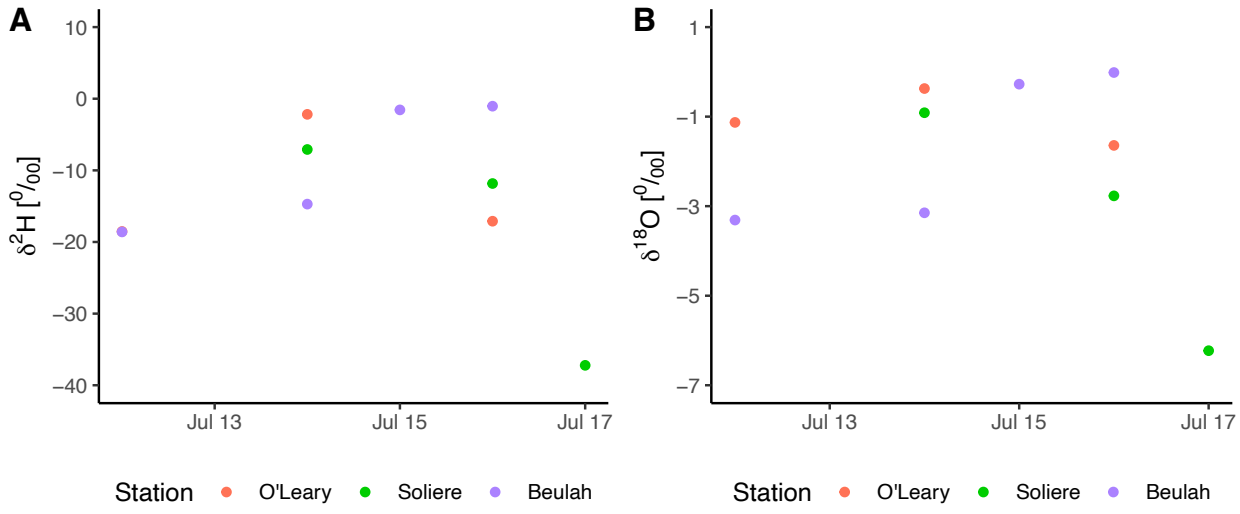

Figure 3.11 Variation in (A)$\delta^{2}H$ and (B) $\delta^{18}O$ from July 12th to July 17th

Once again, this enrichment may be explained by both the formation of precipitation through evapotranspiration and by evaporation that can occur during water's descent through an

atmosphere of low relative humidity, as was the case following the eleven-day dry period. A shift in wind direction was also observed during this time, prompting locally formed clouds to drift west. These factors correspond with the isotopic variation found between stations on July 12th, as the samples became more isotopically depleted with distance west. A convective storm front hailing from the southeast impacted Flagstaff on July 14th, where all precipitation samples were more enriched than July 12th samples. Compared to the O'Leary and Soliere samples, the precipitation collected at the Beulah station was significantly more depleted in both isotopes. However, the Beulah station did not collect precipitation from earlier on in the storm event, as did the other two collectors.

This comparison can be used to highlight a temporal variation in the $\delta^{18}O$ and $\delta^{2}H$ values measured over the evolution of the storm event. The precipitation captured later in the event was more depleted, likely due to the raining out of heavier isotopes during the earlier portion of the storm. Although the Soliere and O'Leary stations were online during the same time frame on July 14th, the O'Leary station received considerably less rain than Soliere. Therefore, the relative enrichment in the O'Leary sample could be explained by the amount effect. Atmospheric moisture from the southeast continued to migrate into Flagstaff on the following day, delivering a small amount of precipitation to the Beulah station that was noticeably more enriched than the previous day's sample. Again, this temporal variation may be caused by the amount effect since the conditions during this event (high temperatures, low humidity, small rainfall amount) were conducive to sub-cloud evaporation.

On July 16th, winds from the southeast continued to transport moisture northwest across Flagstaff. Resultingly, precipitation impacted the Soliere collector first before moving along towards the other stations. The variation in stable isotope delta values between the O'Leary and

Soliere samples is likely due to raining out of the heavier isotopes within the air mass as it progressed eastward. Although the Beulah collector is the furthest station to the west, its sample from July 16th had the highest stable isotope delta values out of the three samples from that day. This contrast can be better understood when considering the fact that Beulah received far less rainfall than the other two stations, as determined by weather radar data. Once again, low relative humidity during light rainfall may have contributed to the enrichment of the Beulah sample. The precipitation collected from Soliere on July 17th was the most isotopically depleted sample within the six-day period. Radar revealed that the sample consisted of very light rainfall originating from the southeast.

3.2.1.3 July 20th to July 30th

Precipitation occurred in Flagstaff every day from July 20th to July 30th. This interval was largely characterized by convective storm systems advancing from the east. During this time span, stable isotope delta values in the samples were strongly correlated with both time and temperature (Figure 3.12).

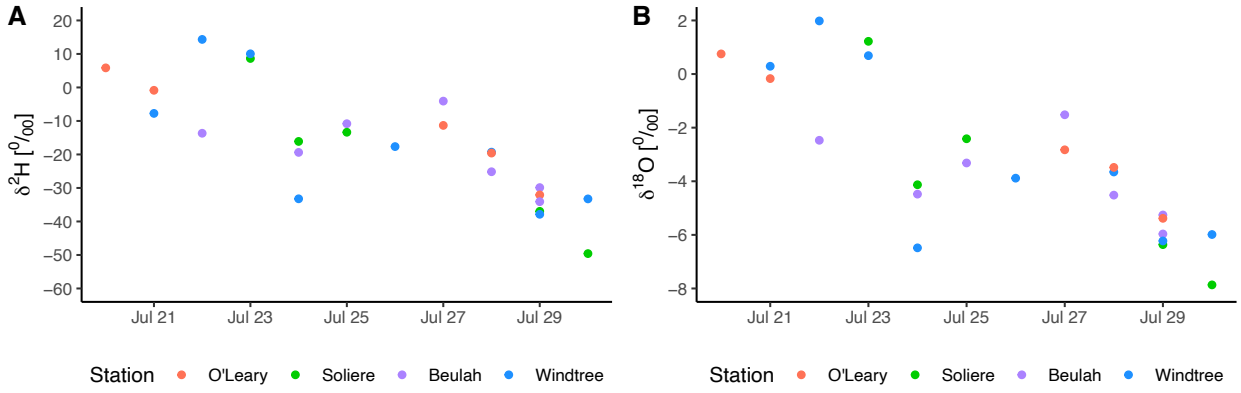

Figure 3.12 Variation in (A)δ^2H and (B) $\delta^{18}O$ from July 20th to July 30th

The precipitation sample collected from O'Leary on July 20th consisted of very light rain brought into Flagstaff from the southwest and was very enriched compared to the Soliere sample

from three days prior. The two samples from the following day had slightly lower delta values with very little variation. Conversely, the precipitation collected on July 22nd exhibited a wide range of isotopic composition amongst the stations. On this date, weather radar revealed that moisture from the southeast drifted over Flagstaff before delivering the earliest portion of the storm event to the Windtree collector. Light rainfall from the latter portion of the event was included in the Beulah sample, which was the most depleted in both stable isotopes. As such, it is reasonable to assume that the Beulah station's position along the storm path may be the cause of the heightened isotopic depletion in the sample.

The samples collected from the July 23rd overnight storm were very isotopically similar, differing by less than 2‰ in both isotopes. All July 24th samples were depleted in $\delta^{18}O$ and $\delta^{2}H$ when compared to the previous day's precipitation, however, the Windtree sample had much lower delta values when compared to the others. This inter-station variability can be better understood by examining the westward trajectory of the air mass over Flagstaff's complex topography. The Soliere station received the earliest part of the precipitation event and had the least depleted sample. As the air mass migrated west, increased rainout occurred over the Mount Elden region before reaching the Windtree collector, resulting in more isotopically depleted precipitation. The portion of the air mass that delivered rainfall to the Beulah collector did not travel over the mountainous area of higher elevation, and therefore was not influenced by the elevation effect.

The July 25th samples collected from the Soliere and Beulah stations were again very isotopically similar and exhibited the same pattern of decreasing $\delta^{18}O$ values as the storm progressed westward. Precipitation continued to flow in from the east on July 26th and July 27th. Samples from July 27th were more enriched than that of July 26th, indicating that some form of

evaporative enrichment may have occurred between the daily samples. Furthermore, the difference in $\delta^{18}O$ and $\delta^{2}H$ values between the July 27th O'Leary and Beulah samples can once again be attributed to the storm's movement over Flagstaff. Weather radar revealed that precipitation moved over Flagstaff from the southeast, where the heaviest rain fell at the O'Leary station. In comparison to the Beulah station, the average rainfall intensity at the O'Leary station was greater by an entire order of magnitude. From this data, it can be inferred that the amount effect may account for the differences between the July 27th samples.

The remainder of the ten-day period was characterized by a trend of increasingly negative stable isotope delta values where inter-station sample variability was generally low. July 28th samples became more depleted with distance west, coinciding with the air mass's trajectory over the collectors. Precipitation isotope data from a large storm on July 29th are used to assess both spatial and temporal variability, since this date includes five samples obtained from four collection stations. To clarify, two samples were collected from the Beulah station at different time intervals. When comparing the two Beulah samples, $\delta^{18}O$ and $\delta^{2}H$ values were observed to decrease over the duration of the storm event. Meanwhile, sample delta values seemed to become more negative with distance north, corresponding to the air mass's movement from southeast to northwest. The most depleted precipitation was captured on the last of the ten-day wet period. On July 30th, an overnight storm from the southeast brought rain to both the Soliere and Windtree stations. The heightened depletion in the Soliere sample is most likely due to the amount effect, given that the Soliere collector received more rain during this event.

3.2.1.4 August 7th to August 19th

The period between August 7th and August 19th was characterized by an overall downward trend in stable isotope delta values (Figure 3.13). A seven-day dry period occurred

before the precipitation event on August 7th, and initial samples were significantly more enriched than those collected on July 30th. Weather radar showed that precipitation in the Windtree sample was produced by light rain throughout the day, in addition to rain from a cloud that developed around an area of higher elevation to the north. The rain collected at Soliere on the following day traveled into Flagstaff from the southeast and had a higher d-excess value (+9.56‰) than the August 7th sample.

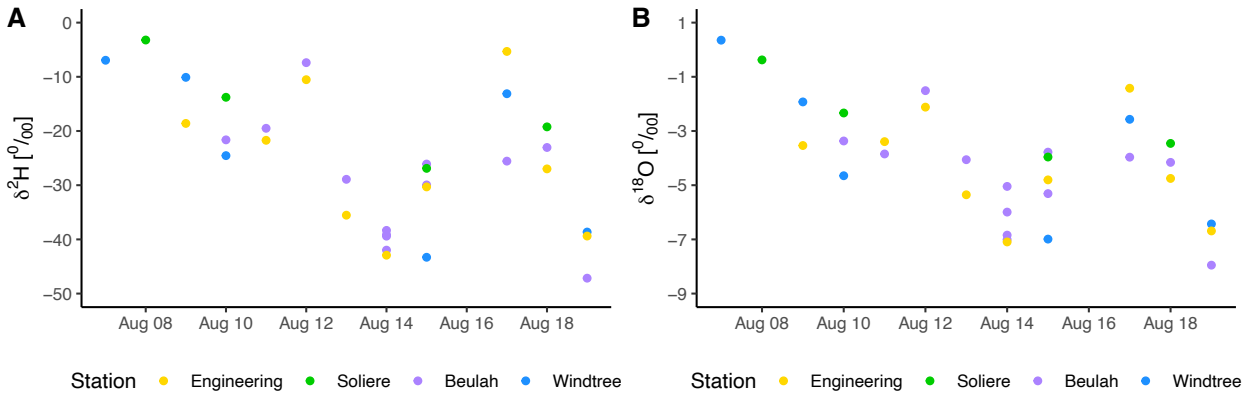

Figure 3.13 Variation in (A)δ^2H and (B) $\delta^{18}O$ from August 7th to August 19th

Precipitation samples from August 9th and 10th were also provided by air masses that migrated into Flagstaff from the southeast. On August 9th, the sample collected at the Engineering station was more depleted than the Windtree sample in both stable isotopes. Additionally, the Windtree sample included light rain from the early morning of August 9th that was not captured in the Engineering sample. Therefore, the relative enrichment of the Windtree sample may be due to the inclusion of light rains from the earlier part of the storm. Furthermore, the August 10th samples from the Soliere and Beulah stations also contained precipitation from the August 9th event. The $\delta^{18}O$ and δ^2H values from these multi-day samples lie between the single-day Windtree samples from August 9th and 10th, demonstrating the gradual depletion in stable isotopes over the evolution of the storm event. Similarly, isotopic values between the

Soliere and Beulah samples became more depleted with distance west, corresponding to the storm's trajectory.

The samples from August 11th and 12th displayed very similar isotopic values between stations, and samples were more enriched over the two-day period. On August 13th and 14th, weather radar showed that precipitation migrated over Flagstaff from the southwest, impacting the Beulah station prior to raining down at the Engineering collector. This information aligns with the daily spatial distribution of stable isotopes amongst stations, which is shown to decrease with distance east. Furthermore, a temporal pattern of δ^2H depletion with storm evolution was observed between the four samples obtained from the Beulah station on August 14th. August 15th precipitation samples, except for Windtree, were generally more enriched than those from the previous day. The Windtree sample's isotopic deviation is most likely due to the inclusion of additional precipitation from August 14th, which is further evidenced by its similarity to the previous day's samples. Once again, a temporal pattern of declining $\delta^{18}O$ and δ^2H values with storm evolution was witnessed between the two Beulah samples collected on August 15th.

The samples collected on August 17th displayed a wide spread of isotopic compositions, with deuterium values ranging from -25.56‰ to -5.32‰. The values of $\delta^{18}O$ and δ^2H were observed to become more negative with precipitation amount, as the Beulah sample had a much larger precipitation volume (+269 mL) and was more depleted than the sample from the Engineering station. The August 18th samples all shared similar stable isotope delta values, which generally decreased from the previous day. The Soliere sample was the most enriched in both $\delta^{18}O$ and δ^2H, likely because it also contained precipitation from the August 17th storm front. Delta values in the other two August 18th samples declined with distance to the northeast, demonstrating a rainout effect as the storm rolled over Flagstaff from the southwest. On August

19th, the samples from Engineering and Windtree stations were very isotopically similar, while the Beulah sample was more depleted. Weather radar revealed that the Beulah station also experienced a significantly higher average intensity of rainfall during the collection period, which may have contributed to its more negative delta values.

3.2.1.5 August 21st to August 27th

The samples collected from August 21st to 27th did not display an obvious trend in stable isotope delta values (Figure 3.14).

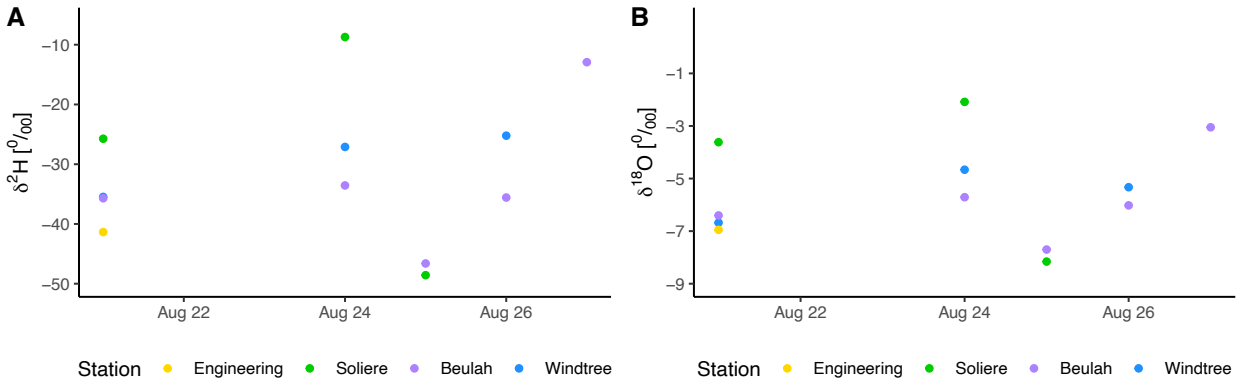

Figure 3.14 Variation in (A)δ2H and (B) δ18O from August 21st to August 27th

Weather radar from August 21st indicated that local evapotranspiration likely contributed the development of clouds in the area, which were observed to grow locally rather than drift into Flagstaff. Furthermore, the earliest portion of that day's precipitation event occurred over the Soliere collector, whose sample was also the most isotopically enriched. When comparing the samples from the other three stations, $\delta^{18}O$ values were observed to decrease with increasing precipitation amount. August 24th samples were more enriched than samples from the previous precipitation event. Once again, weather radar suggested that precipitation may have been produced by local evapotranspiration in the area. Similar to the previous storm event, the earliest and lightest portion of precipitation occurred at the Soliere collector. Later in the day, a large

storm developed within the Flagstaff area that supplied heavy rain to the Windtree collector before migrating south towards the Beulah station. Overall, the August 24th samples illustrate isotopic depletion over the progression of the storm event.

Samples from August 25th were isotopically alike and were significantly more depleted in stable isotopes when compared to the previous day's results. The August 25th precipitation belongs to a storm front that traveled over Flagstaff from west to east. Correspondingly, samples were more depleted in both $\delta^{18}O$ and $\delta^{2}H$ with distance eastward. August 26th and 27th precipitation samples were increasingly enriched over the two days. On August 26th, the Windtree sample had higher stable isotope delta values while also receiving the earlier portion of the storm. It is likely that intense rainout occurred within the air mass prior to its arrival at the Beulah station, where only a small amount of rainfall was collected. This rainout effect may explain the variation seen within the two samples from this day.

3.2.1.6 September 10th to September 23rd

The two-week dry period occurring between August 27th and September 10th was broken by a storm system migrating from the southeast. Figure 3.15 displays the station results from September 10th to 23rd. Samples from September 10th had significantly lower stable isotope delta values when compared to the most recent event in August.

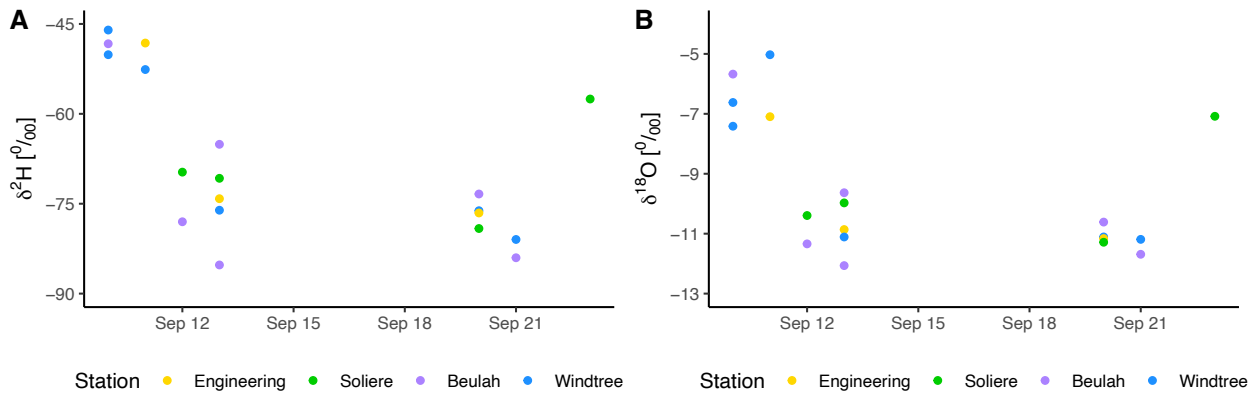

Figure 3.15 Variation in (A)δ^2H and (B) $\delta^{18}O$ from September 10th to September 23rd

A pattern of decreasing $\delta^{18}O$ and δ^2H values with storm evolution can be identified when examining the Windtree station's results from the first day in this time series. On September 10th, the most enriched Windtree sample was collected during the early portion of the storm event while the Windtree sample from later in the event was more depleted. Additionally, stable isotope delta values were observed to decrease with the station's distance north, consistent with the storm's progression over Flagstaff. A comparison of the d-excess values found in September 11th precipitation revealed that the samples followed the same trend of isotopic depletion with distance north. The samples collected on September 12th and 13th displayed similar ranges in isotopic composition. This precipitation collected on September 12th was largely from a southwesterly storm that occurred overnight, leading into September 13th. Although winds were directing clouds from west to east, the earliest portion of the precipitation event began at the Soliere station. The Beulah station received precipitation from air masses that followed, which may explain the more negative delta values found in the Beulah sample.

The two Beulah samples from September 13th demonstrate temporal variability in the isotopic ratios of precipitation from a single event. This pattern is identical to what was observed in the Windtree samples from September 10th, where $\delta^{18}O$ and δ^2H values declined over the

duration of the event. Once again, a storm front from the southwest was responsible for September 13th precipitation. This storm system impacted the Beulah station first, whose initial sample represents the most enriched precipitation on this date. The samples from the other three stations displayed the amount effect, the observation that precipitation becomes more depleted as precipitation amount increases. Another seven-day dry period followed the September 13th event.

The precipitation captured on September 20th and 21st was produced by an air mass migrating through Flagstaff from the southwest, during which precipitation samples were more depleted with time. Minimal variation was seen between the individual sample's collected on these two days. Note that the samples collected from Engineering and Soliere contain precipitation from both September 20th and 21st, which is supported by their isotopic values relative to the other samples. The difference in isotopic contents amongst the Beulah and Windtree samples is credited to the storm's trajectory over the area. To enumerate, the Windtree station received morning precipitation on September 21st that was not included in the Beulah sample, which may be the cause of the Windtree sample's slightly higher delta values. September 23rd precipitation once again moved over Flagstaff from the southwest, resulting in a sample that was isotopically enriched as compared to the samples from two days prior.

3.2.1.7 October 2nd to October 6th

The rainfall received on October 2nd marked the beginning of the autumn sampling period. Figure 3.16 shows the spread in $\delta^{18}O$ and $\delta^{2}H$ values from October 2nd to October 6th. Samples from October 2nd had significantly higher $\delta^{18}O$ and $\delta^{2}H$ values when compared to the previous precipitation event that occurred nine days earlier. Weather radar from this day indicated that local evapotranspiration may have contributed to the precipitation in the area.

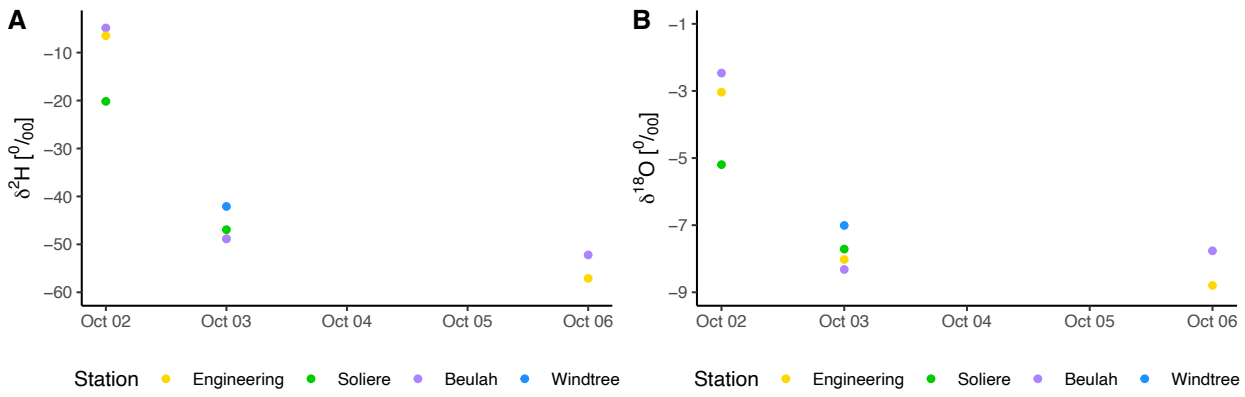

Figure 3.16 Variation in (A)δ^2H and (B) $\delta^{18}O$ from October 2nd to October 6th

The Soliere station experienced the largest amount of precipitation on this day and was the most depleted in both stable isotopes. The samples from the Beulah and Engineering stations were very isotopically similar, however the Beulah sample had slightly higher delta values. The samples were observed to get more isotopically depleted with distance east. Precipitation samples on the following day, October 3rd, exhibited a small range of more negative delta values. This precipitation belonged to a large overnight storm hailing from the northwest, which peaked at the Windtree station. The stable isotope delta values and d-excess in the samples were observed to decrease with average rainfall intensity at each station ($\delta^{18}O$, $r = 0.91$, $p = 0.087$). Peaks in rainfall intensity were observed at the Windtree and Soliere collectors, while the Beulah and Engineering stations primarily received lighter rain. Three days ensued before a small precipitation event occurred on the night of October 6th, moving into Flagstaff with winds from the east. Little variability was seen between the October 6th samples.

3.2.1.8 October 15th to October 22nd

Precipitation samples collected from October 15th to October 22nd primarily displayed the same spatial trend of isotopic depletion with distance to the west (Figure 3.17).

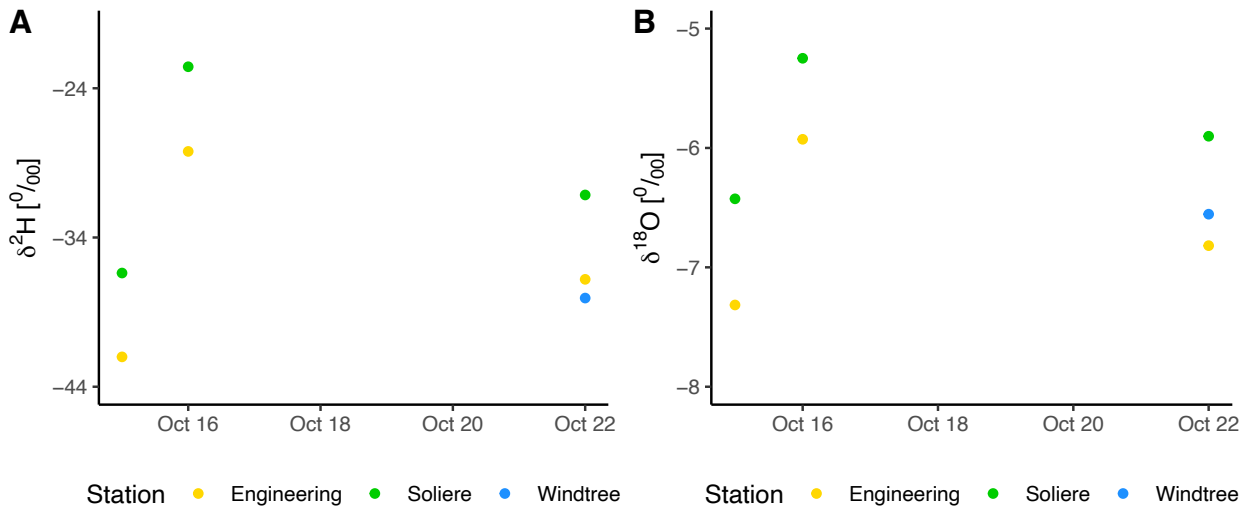

Figure 3.17 Variation in (A)δ^2H and (B) $\delta^{18}O$ from October 15th to October 22nd

The precipitation samples collected on October 15th and 16th were produced by a storm front emerging from the southeast. On both days, the Soliere samples were richer in $\delta^{18}O$ and δ^2H when compared to the Engineering samples. Additionally, weather radar data revealed that the average rainfall intensity during both days was higher at the Engineering station than at the Soliere station. Rather than becoming more depleted with time, precipitation samples were observed to become more enriched from October 15th to October 16th. After a period of six precipitation-free days, weather radar indicated that precipitation on October 22nd was likely produced from local evapotranspiration. The October 22nd samples were less rich in stable isotopes as compared to the October 16th samples. Amongst these samples, the Soliere station showed the highest values of in $\delta^{18}O$ and δ^2H and was the first station to receive rainfall during the event.

3.2.1.9 November 2nd to November 9th

The final period of precipitation collection occurred from November 2nd to November 9th (Figure 3.18), following more than two weeks without precipitation in Flagstaff.

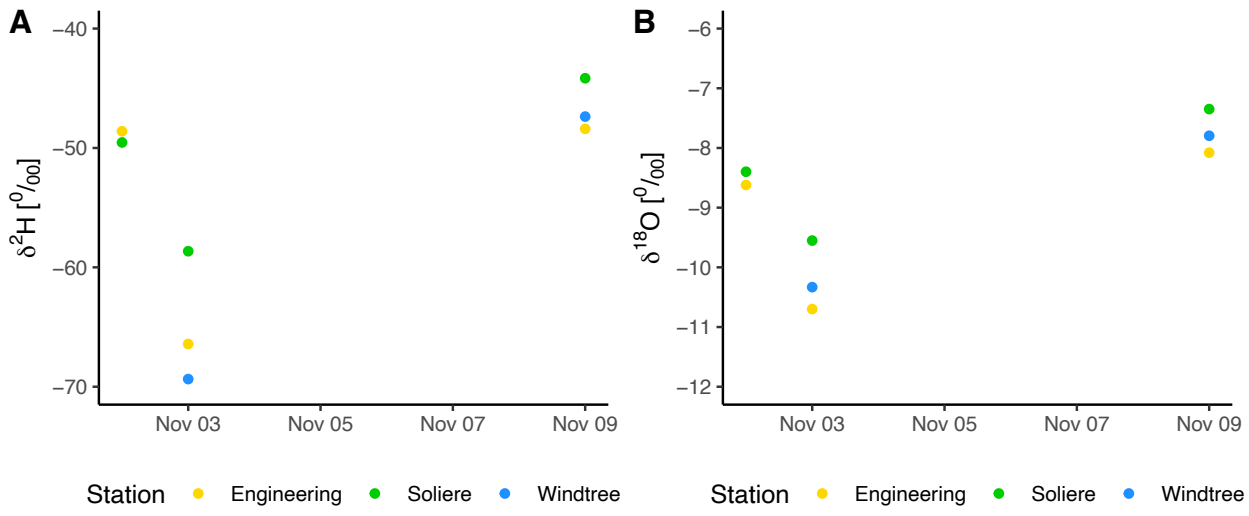

Figure 3.18 Variation in (A)δ^2H and (B) $\delta^{18}O$ from November 2nd November 9th

The samples collected on November 2nd demonstrated very low inter-station variability between delta values and were more depleted than the samples from weeks prior. Weather radar showed that the precipitation from this event moved into Flagstaff from the southwest. November 3rd samples exhibited a wider range of stable isotope delta values. When compared to the Windtree and Engineering stations in west Flagstaff, the Soliere station received a significantly smaller amount of precipitation and was the most enriched sample. November 9th precipitation samples were provided by a large storm that migrated into Flagstaff from the northwest. These samples displayed a small range in isotopic content, and samples were more depleted with increasing rainfall amount.

4 Discussion

Since all sampling stations were located within an elevation range of about 300 feet, isotopic effects due to elevation were not considered. The isotopic results from this study were similar to those published by Beisner et al. [5] for their Flagstaff station at 7,100 feet in elevation. The

LMWL determined by this study had a lower slope and intercept value than the 2003 – 2014 data from Beisner et al. [5], however, the datasets are not entirely comparable due to the differences in sample collection methods (composite seasonal sampling versus event-scale sampling) and sampling periods (the present study did not include precipitation from April – May). The mean d-excess found during the present study was 8.48‰, lower than the mean d-excess of 10.03‰ previously determined by Beisner et al. [5]. Likewise, the mean $\delta^{18}O$ and $\delta^{2}H$ values from the late monsoon season ($\delta^{2}H$ = -44.28‰, $\delta^{18}O$ = -6.80‰) were in agreement with the results found by Tulley-Cordova et al. [21] for the NAM precipitation samples collected on the Navajo Nation from 2014 to 2017.

4.1.1 Temporal Trends

Seasonal variations of stable isotope delta values were consistent with previously observed trends in the composition of precipitation in Arizona, which correspond to the source of moisture and temperature of condensation. To clarify, summer precipitation is normally more isotopically enriched than winter precipitation because it may include more recycled water that is condensed at a higher temperature and is more likely to fall subject to sub-cloud evaporation during descent [7]. On the contrary, winter (or autumn in this case) precipitation is more depleted because it is condensed at cooler temperatures from mid-latitude frontal systems that convey moisture from the Pacific Ocean [7]. These seasonal shifts in atmospheric circulation features were also verified through visual observation of weather radar imaging.

The analysis of seasonal, weekly, and daily isotopic data allowed for a multi-tiered investigation into temporal trends. Access to precipitation data from event-based collection grants the opportunity to evaluate short-term isotopic variability, which differs from the standard monthly collection interval required for GNIP datasets. For instance, seasonal mean d-excess

values were observed to increase with time, but the same pattern is not particularly evident when breaking the data down on a week-to-week basis (Table 3.3, Table 3.4). Resultingly, the fluctuations in weekly mean d-excess values were overwhelmingly found to correspond with ambient air temperature (Figure 3.8). Likewise, weekly mean $\delta^{18}O$ values gradually decreased over the course of the late monsoon season. The opposite was true of mean $\delta^{18}O$ values during the first three weeks of the early monsoon, which displayed an increasing trend. These temporal tendencies are again strongly correlated with ambient temperature, which increased during the beginning of the early monsoon and decreased at the end of the monsoon. These weekly data revealed isotopic trends that could not be identified with monthly data alone. Therefore, high frequency precipitation sampling has proven to be valuable for identifying climatic correlations that are not obvious when only considering monthly or seasonal averages.

Moreover, the use of daily data enables deeper levels of analysis by revealing storm events that are highly influential on weekly and monthly isotopic measurements. For example, the mean stable isotope delta values during the first week of Autumn were highly influenced by a single event on October 2nd that caused the average to greatly increase. In addition to the trends identified on a seasonal or weekly basis, temporal patterns were also observed between the daily data. In general, precipitation samples containing water from the earlier portion of the storm event were less depleted than those from later in the storm. This trend of gradually more negative stable isotope values with storm evolution is consistent with the continental effect, where the upwind rainout of heavier isotopes results in isotopically depleted precipitation downwind [7]. Furthermore, analysis of event-based data showed that wide ranges of stable isotope ratios were observed over relatively short timescales. These isotopic differences can provide enhanced

insight into atmospheric moisture transport in an area but are typically masked by monthly and weekly averages.

4.1.2 Spatial Trends

Although all sampling stations were located within a 3.5-mile radius, the isotopic composition of samples typically varied from station to station. This variation was often correlated with the trajectory of the moisture-bearing air mass over Flagstaff and the resultant distribution of precipitation throughout the area. As was previously mentioned, samples were normally observed to become more depleted over the duration of the storm event. Likewise, precipitation samples were often found to be more depleted with distance along the storm's pathway. This result was observed between samples from each of the multi-day groupings, and again, this pattern of depletion can be attributed to the continental effect. Furthermore, the relative enrichment of upwind samples may have been exacerbated by sub-cloud evaporation that is more likely to occur during the earlier portion of a storm event when relative humidity is at its lowest [25]. A combination of these two influencing factors likely caused the isotopic differences that were observed in samples from several events.

On the same note, precipitation samples from light rainfall were typically more enriched than those that contained water from heavy parts of the storm event. Although this "amount effect" was not observed when analyzing the dataset as a whole, the impact of precipitation amount was noticed when examining of the variability found between samples from a single event. In fact, the amount effect was observed in samples from multiple dates, including July 14th, July 27th, July 30th, August 17th, August 21st, September 13th, and October 2nd, and more. There were no significant differences in the distribution of stable isotope delta values among stations (Figure

3.9), which was expected given the negligible elevation change between collectors and the proximity of the collection stations.

5 Design of Precipitation Collection Devices for Future Event-Scale Sampling in Flagstaff

The existing precipitation collection network was improved upon in April 2023, at the beginning of the next rainfall collection season. New collection devices were constructed using the method by Gröning et. al [26], which essentially eliminates the risk of evaporation during rain sampling by reducing the amount of water surface exposed to the atmosphere. This is accomplished by installing a narrow soft polypropylene plastic tube to convey water from the collection funnel down to the bottom of the sample bottle. Only a small amount of rainfall is needed for the water level in the bottle to rise into the plastic tube, stopping gas transfer between the bottle's headspace and the open atmosphere. Furthermore, the collection bottle is thermally isolated from sunlight by a double container construction made of PVC pipe. The top of the sample bottle is permanently attached to the inner shell of the collector so that the operator only has to un-screw the bottle, allowing for efficient bottle replacement. The collection funnel is then mounted to the sampling device via a 3-D printed piece that is used to join the funnel and internal plastic tube.

Additionally, the top of the sample bottle is fitted with an external pressure equilibrium tube to keep the air pressure within the bottle at atmospheric levels. This tube is wrapped around the collector's inner shell, where the outer container shields it from sunlight. The external tube's total volume is set to be about 10% of the bottle's volume to allow for pressure fluctuations of ± 50 hPa to occur without significant moisture exchange with the atmosphere. In a situation of

decreasing atmospheric pressure, this prevents water from rising out of the collector through the inner plastic tube, where it could reach the funnel and become subject to evaporation. The outer shell of the collector is fashioned with two eyebolts so that it may be vertically mounted to free-standing rebar. The dimensions of the collector (Table 5.1) were chosen to prevent overflow from Flagstaff's maximum storm event, using data from 2017 to 2021.

Table 5.1 Event-sized Precipitation Collector

Specification	**Value**	**Unit**
Bottle Volume	500	mL
Funnel Diameter	4	in
Inner PVC Shell Diameter	4	in
Outer PVC Shell Diameter	6	in
¼" Inner Diameter Internal Tube	25	cm
1/8" Inner Diameter External Tube	6.3	m

The new sampling devices will improve the quality of isotopic data collection by essentially diminishing the risk of post-collection evaporation. These collectors will be employed at the Windtree, Beulah, Engineering, and Soliere collection stations, as well as at two additional stations of higher elevations. The two new collection stations will be located north of the city of Flagstaff, at elevations of around 8,000 and 9,000 feet. Collecting precipitation from a range of elevations will allow for future analysis of the elevation effect on stable isotope delta values in Flagstaff. Furthermore, continuing sample collection at existing stations will allow for temporal comparisons of site-specific stable isotope data on broader timescales than is presented in this work.

6 Implementing a Citizen-Science Precipitation Collection Network

A citizen-science precipitation collection network has been set up with the intent of expanding sample collection in Coconino County. The establishment of this network provides the local community with an opportunity to contribute to hydrological research and increases sampling potential. Furthermore, expanding the sampling network across the city of Flagstaff will increase the range of data collection, allowing for enhanced analysis of spatial and temporal variability in stable isotope delta values. A website was developed to inform the public of the project and functions as a sign-up platform for managing a collector. Collection devices (as described in the previous section) are installed at participant's residences by project personnel. Participants are given instructions for proper collection and may collect on a voluntary basis. After collection, participants can turn in their samples at a designated drop-off location within Northern Arizona University's Engineering Building.

Engaging the local community through citizen-science benefits both the project and the people of Flagstaff in many ways. Perhaps the most obvious is that it increases public engagement, which builds trust between the scientific community and society [27]. Developing mutual trust and respect between scientists and the public is especially important in today's post-truth world [28]. Additionally, participation in the citizen-science network can be used as an educational opportunity to teach students in local schools or environmental programs about hydrologic research and spark interest in the field. Likewise, involvement in citizen-science is known to increase knowledge and raise awareness of issues related to the study topic. This enhanced level of awareness and improved scientific literacy amongst community members can result in behavioral changes like more environmentally conscious behavior or increased political participation [28].

In this project, for example, citizen-scientists will likely learn about Flagstaff's water resource challenges that isotopic data analysis can assist in. As a result of heightened awareness about water resource issues, participants may be inclined to display more environmentally responsible behavior, such as trying to conserve water in their daily lives. Alternatively, citizen-scientists may be more motivated to engage in civic matters related to water resources planning and decision-making processes. These scenarios illustrate how the democratization of scientific research can benefit all parties involved, as is the goal in launching the citizen-science precipitation collection network.

7 Conclusion

The LMWL determined by this research was similar to the summer equation previously found by Beisner et al. [5] for their Flagstaff station. Likewise, late monsoon precipitation exhibited mean stable isotope delta values that were close to the values published by Tulley-Cordova et al. [21] for NAM precipitation in a region that is directly northeast of Flagstaff. Ultimately, the variations in the isotopic composition of precipitation samples reflect differences in storm origin, atmospheric flow paths, and ambient temperature. Early monsoon precipitation samples were typically the most enriched in both stable isotopes and generally followed an increasing trend with both time and temperature. Compared to the latter seasons, the relative enrichment of early monsoon samples coincides with the rising temperatures and arid conditions present during the sampling period. In contrast, late monsoon precipitation samples were increasingly depleted over the duration of the sampling period and had the lowest mean value of deuterium. Autumn precipitation samples shared the highest d-excess values and demonstrated

the lowest spread in isotopic composition. Overall, the peaks in daily mean stable isotope values were observed to become more negative as the seasons progressed.

Additionally, weekly mean d-excess values showed a strong negative correlation with temperature. Since temperatures generally decreased over the duration of the sampling period, d-excess is also strongly correlated with time. The use of event-scale precipitation sampling revealed short-term spatial and temporal variations in isotopic ratios. The isotopic composition of samples from a single event were typically similar, however in some cases, precipitation samples from an event differed by up to 28.01‰ and 4.45‰ in $\delta^{2}H$ and $\delta^{18}O$, respectively. These short-term variations were investigated with the help of weather radar data that illustrated atmospheric circulation patterns and, to a degree, enabled moisture source tracing. Samples were largely shown to become less enriched in stable isotopes as the precipitation event evolved due to the gradual raining out of heavier isotopes. Identically, downwind samples were typically more depleted than those that were impacted by the storm prior. Although these patterns were common within the dataset, further investigation is needed to better understand the instances where rainout effects did not occur as expected. Likewise, future analysis should aim at identifying a method to distinguish between precipitation produced by local evapotranspiration and precipitation that has migrated into the area from oceanic waters. Lastly, future sampling efforts should prioritize the use of consistent sampling periods between stations so that all samples belonging to an event are on the timescale. Establishing a specified collection interval for precipitation sampling reduces the ambiguity associated with interpreting data from varying time frames.

The work presented here is significant to isotopic research in Northern Arizona in several ways. First, the establishment of the current precipitation collection network has created a

baseline dataset that can be utilized in long-term temporal comparisons in the forthcoming years. Even more so, the intended expansion of the network will augment sample collection and facilitate new pathways of analysis (the elevation effect, for example). Second, this dataset represents the first event-scale sampling campaign that has been conducted for isotopic analysis of precipitation in Flagstaff. As previously mentioned, event-scale sampling adds value to monthly or seasonal data by demonstrating short-term spatial and temporal variability in the isotopic composition of precipitation. Third, the use of a citizen-science precipitation sampling network for the analysis of stable isotopes is unique to Arizona and may motivate similar projects in other regions of the state. This not only aids in data collection, but also works to bring awareness to local hydrological challenges that may benefit from the application of isotopic analysis.

Finally, and most importantly, stable isotope data from precipitation can be analyzed in conjunction with groundwater and streamflow data to answer important questions about the hydrology in a watershed. For example, stable isotope data can be used to quantify the contributions of seasonal precipitation to subsurface water resources or may be used to assess the impact of wildfire burn scares on runoff generation. The results from such analyses can then be employed to make predictions and inform water resource management decision-making. Although this type of combined analyses were not within the scope of this research, this project has essentially laid the foundation for future stable isotope studies by providing baseline precipitation data for the area and establishing an avenue for continued isotope data collection.

8 Bibliography

[1] M. A. Crimmins, "ARIZONA AND THE NORTH AMERICAN MONSOON SYSTEM," *Arizona Cooperative Extension: College of Agriculture and Life Sciences,* September 2006.

[2] A. M. Meadow, J. L. Weiss, S. LeRoy and L. Keith, "Climate Profile for the City of Flagstaff, Arizona," Climate Assessment of the Southwest (CLIMAS), Tucson, Arizona, 2018.

[3] C. Kendall and E. A. Caldwell, "Fundamentals of Isotope Geochemistry," in *Isotope Tracers in Catchment Hydrology*, Elsevier Science, 1998, p. 51.

[4] International Atomic Energy Agency, "Global Network of Isotopes in Precipitation (GNIP)," [Online]. Available: https://www.iaea.org/services/networks/gnip. [Accessed 3 April 2023].

[5] K. R. Beisner, N. V. Paretti and R. S. Tucci, "Analysis of Stable Isotope Ratios (δ18O and δ2H) in Precipitation of the Verde River Watershed, Arizona, 2003 through 2014," U.S. Geological Survey Open-File Report, Reston, 2016.

[6] K. W. Blasch and J. R. Bryson, "Distinguishing Sources of Ground Water Recharge by Using d2H and d18O," *Ground Water,* vol. 45, no. 3, pp. 294-308, 2007.

[7] N. L. Ingraham, "Chapter 3: Isotopic Variations in Precipitation," in *Isotope Tracers in Catchment Hydrology*, Elsevier Science, 1998, pp. 88-118.

[8] W. Dansgaard, "Stable isotopes in precipitation," *Tellus,* vol. 16, no. 4, pp. 436-468, 1964.

[9] L. Merlivat and J. Jouzel, "Global climatic interpretation of the deuterium-oxygen 18 relationship for precipitation," *Journal of Geophysical Research Atmospheres,* vol. 84, pp. 5029-5033, 1979.

[10] S. Pfahl and H. Sodemann, "What controls deuterium excess in global precipitation?," *Climate of the Past,* vol. 10, pp. 771-781, 2014.

[11] K. Froehlich, J. J. Gibson and P. Aggarwal, "DEUTERIUM EXCESS IN PRECIPITATION AND ITS CLIMATOLOGICAL SIGNIFICANCE," *Journal of Geophysical Research,* 2002.

[12] H. Craig, "Isotopic Variations in Meteoric Waters," *Science,* vol. 133, no. 3465, pp. 1702-1703, 1961.

[13] M. Staudenmaier, R. Preston and P. Sorenson, "Climate of Flagstaff, Arizona," National Oceanic and Atmospheric Administration, Flagstaff, 2009.

[14] J. Lisonbee, A. Sheffield, A. Lang, E. Ossowski, K. Satalino, S. McAfee, E. Saffell, D. McEvoy, D. Simeral, P. Iniguez, V. Murphy, A. Tardy, J. Casola and M. Crimmins, "North American Monsoon and Drought Relief," National Integrated Drought Information System, 30 June 2022. [Online]. Available: https://www.drought.gov/drought-status-updates/north-american-monsoon-and-drought-relief. [Accessed 14 February 2023].

[15] D. K. Adams and A. C. Comrie, "The North American Monsoon," *Bulletin of the American Meteorological Society,* pp. 2197-2213, 19 May 1997.

[16] National Weather Service, "What is ENSO?," National Oceanic and Atmospheric Administration, [Online]. Available: https://www.weather.gov/mhx/ensowhat. [Accessed 20 March 2023].

[17] K. Velev, "El Niño/La Niña Watch & PDO," NASA Jet Propulsion Laboratory , [Online]. Available: https://sealevel.jpl.nasa.gov/data/el-nino-la-nina-watch-and-pdo/pacific-decadal-oscillation-pdo/. [Accessed March 20 2023].

[18] National Oceanic and Atmospheric Administration, "Flagstaff Pulliam Airport Climate Data," Flagstaff, 2022.

[19] T. M. Luong, C. L. Castro, H.-I. Chang, T. Lahmers, D. K. Adams and C. A. Ochoa-Moya, "The More Extreme Nature of North American Monsoon Precipitation in the Southwestern United States as Revealed by a Historical Climatology of Simulated Severe Weather Events," *Journal of Applied Meteorology and Climatology,* vol. 56, no. 9, pp. 2509-2529, 2017.

[20] T. M. Lahmers, C. L. Castro, D. K. Adams, Y. L. Serra, J. J. Brost and T. Luong, "Long-term changes in the climatology of transient inverted troughs over the North American monsoon region and their effects on precipitation," *Journal of Climate,* vol. 29, no. 17, pp. 6037-6064, 2016.

[21] C. L. Tulley-Cordova, A. L. Putman and G. J. Bowen, "Stable Isotopes in Precipitation and Meteoric Water: Sourcing and Tracing the North American Monsoon in Arizona, New Mexico, and Utah," *Water Resources Research,* vol. 57, 2021.

[22] L. Metcalf, *Ground water - surface water interactions in the lower virgin river area, Arizona and Nevada,* UNLV, 1995.

[23] G. I. Smith, I. Friedman, H. Klieforth and K. Hardcastle, "Areal Distribution of Deuterium in Eastern California Precipitation, 1968–1969," *Journal of Applied Meteorology,* vol. 18, no. 2, pp. 172-188, 1979.

[24] S. Ansari, C. Hutchins, S. Del Greco, N. Stroumentova and M. Phillips, "THE WEATHER AND CLIMATE TOOLKIT," in *American Geophysical Union Fall Meeting*, 2010.

[25] J. R. Gat and R. Gonfiantini, "Stable Isotope Hydrology: Deuterium and Oxygen-18 in the Water Cycle," International Atomic Energy Agency, Vienna, 1981.

[26] M. Gröning, H. O. Lutz, Z. Roller-Lutz, M. Kralik, L. Gourcy and L. Pöltenstein, "A simple rain collector preventing water re-evaporation dedicated for d18O and d2H analysis of cumulative precipitation samples," *Journal of Hydrology,* Vols. 448-449, pp. 195-200, 2012.

[27] P. M. Groffman, C. Stylinki, M. C. Nisbet, C. M. Duarte, R. Jordan, A. Burgin, M. A. Previtali and J. Coloso, "Restarting the conversation: challenges at the interface between ecology and society," *Frontiers in Ecology and the Environment,* vol. 8, no. 6, pp. 284-291, 2010.

[28] D. W. Walker, M. Smigaj and M. Tani, "The benefits and negative impacts of citizen science applications to water as experienced by participants and communities," *WIREs Water,* vol. 8, 2020.

9 Appendices

9.1 Appendix A: Sample Data

Table 9.1 Early Monsoon Sample Data: 6/23/2022 – 7/16/2022

Station	Event Date	Start Date	End Date	δ^2H, ‰	$\delta^{18}O$, ‰	d-excess, ‰	Amount, in.
O'Leary	6/23/22	6/23/22 6:00	6/24/22 12:05	-61.75	-7.96	1.91	0.010
Soliere	6/23/22	6/23/22 5:55	6/24/22 6:30	-65.93	-8.42	1.42	0.010
Soliere	6/24/22	6/24/22 6:45	6/25/22 11:30	-65.52	-8.36	1.34	0.070
Soliere	6/26/22	6/25/22 11:45	6/26/22 16:00	-39.26	-5.44	4.29	0.010
Windtree	6/26/22	6/25/22 12:20	6/26/22 15:00	-57.37	-8.97	14.38	0.080
Soliere	6/30/22	6/26/22 16:00	7/1/22 6:30	-34.45	-5.02	5.68	0.750
O'Leary	6/30/22	6/30/22 9:30	7/1/22 10:35	-34.83	-5.43	8.64	0.190
O'Leary	7/1/22	7/1/22 10:40	7/2/22 11:05	-40.45	-4.24	-6.55	0.030
Soliere	7/1/22	7/1/22 6:40	7/2/22 11:15	-54.83	-7.82	7.77	0.270
O'Leary	7/12/22	7/11/22 10:55	7/12/22 11:00	-18.53	-1.13	-9.50	0.032
Beulah	7/12/22	7/11/22 15:00	7/12/22 11:30	-18.60	-3.31	7.89	0.050
O'Leary	7/14/22	7/12/22 11:00	7/15/22 11:35	-2.18	-0.37	0.80	0.190
Soliere	7/14/22	7/12/22 6:30	7/15/22 6:30	-7.09	-0.91	0.22	0.243
Beulah	7/14/22	7/12/22 11:30	7/14/22 18:00	-14.71	-3.15	10.47	0.190
Beulah	7/15/22	7/14/22 18:00	7/16/22 18:00	-1.56	-0.28	0.64	0.400
Beulah	7/16/22	7/16/22 18:00	7/17/22 15:15	-1.04	-0.01	-0.93	0.070
Soliere	7/16/22	7/15/22 6:30	7/17/22 15:00	-11.84	-2.77	10.32	0.070

Table 9.2 Early Monsoon Sample Data: 7/16/2022 – 7/28/2022

Station	Event Date	Start Date	End Date	δ^2H, ‰	$\delta^{18}O$, ‰	d-excess, ‰	Amount, in.
O'Leary	7/16/22	7/15/22 11:35	7/17/22 14:05	-17.10	-1.64	-3.96	0.021
Soliere	7/17/22	7/17/22 15:00	7/18/22 11:00	-37.22	-6.23	12.60	0.080
O'Leary	7/20/22	7/20/22 8:00	7/21/22 11:00	5.85	0.75	-0.17	0.010
O'Leary	7/21/22	7/21/22 11:00	7/22/22 13:05	-0.85	-0.17	0.51	0.071
Windtree	7/21/22	7/20/22 15:00	7/21/22 17:00	-7.74	0.29	-10.07	0.014
Windtree	7/22/22	7/21/22 17:00	7/23/22 15:30	14.33	1.98	-1.52	0.130
Soliere	7/23/22	7/17/22 15:00	7/24/22 10:15	8.65	1.22	-1.11	0.061
Beulah	7/22/22	7/21/22 16:00	7/23/22 15:00	-13.67	-2.47	6.10	0.270
Windtree	7/23/22	7/23/22 15:30	7/24/22 12:30	10.04	0.69	4.55	
Soliere	7/24/22	7/24/22 10:20	7/25/22 6:30	-16.11	-4.13	16.93	0.243
Beulah	7/24/22	7/24/22 8:00	7/25/22 8:00	-19.39	-4.48	16.46	0.400
Windtree	7/24/22	7/24/22 12:30	7/25/22 15:00	-33.23	-6.48	18.64	0.010
Beulah	7/25/22	7/25/22 8:00	7/26/22 8:00	-10.82	-3.32	15.72	0.010
Soliere	7/25/22	7/25/22 6:40	7/26/22 6:45	-13.37	-2.41	5.94	0.039
Windtree	7/26/22	7/25/22 15:00	7/27/22 9:00	-17.65	-3.88	13.42	0.870
Beulah	7/27/22	7/27/22 8:00	7/28/22 11:00	-4.08	-1.52	8.07	0.870
O'Leary	7/27/22	7/27/22 11:00	7/28/22 7:30	-11.33	-2.83	11.29	0.030
Windtree	7/28/22	7/27/22 9:00	7/29/22 7:30	-19.31	-3.65	9.92	0.110
O'Leary	7/28/22	7/28/22 7:30	7/29/22 13:05	-19.59	-3.48	8.27	0.210
Beulah	7/28/22	7/28/22 11:00	7/29/22 11:00	-25.15	-4.52	10.99	0.060

Table 9.3 Early Monsoon Sample Data: 7/29/2022 – 8/13/2022

Station	Event Date	Start Date	End Date	δ^2H, ‰	$\delta^{18}O$, ‰	d-excess, ‰	Amount, in.
O'Leary	7/29/22	7/29/22 7:30	7/30/22 12:30	-32.08	-5.38	10.99	0.070
Beulah	7/29/22	7/29/22 15:15	7/30/22 8:00	-34.09	-5.97	13.64	0.607
Soliere	7/29/22	7/29/22 7:15	7/30/22 7:15	-36.97	-6.36	13.93	0.230
Windtree	7/29/22	7/29/22 7:30	7/30/22 7:30	-37.86	-6.23	11.95	0.070
Windtree	7/30/22	7/30/22 7:30	8/1/22 9:00	-33.26	-5.99	14.63	0.630
Soliere	7/30/22	7/30/22 7:15	8/1/22 8:45	-49.59	-7.87	13.34	0.850
Windtree	8/7/22	8/7/22 7:30	8/8/22 8:00	-6.95	0.35	-9.76	0.010
Soliere	8/8/22	8/8/22 6:30	8/9/22 11:15	-3.21	-0.38	-0.20	0.010
Windtree	8/9/22	8/8/22 8:00	8/10/22 9:50	-10.10	-1.93	5.31	0.040
Engineering	8/9/22	8/9/22 8:00	8/10/22 9:00	-18.60	-3.54	9.69	0.010
Soliere	8/10/22	8/9/22 11:15	8/11/22 6:45	-13.78	-2.34	4.90	0.010
Beulah	8/10/22	8/9/22 9:00	8/11/22 8:00	-21.63	-3.37	5.31	0.010
Windtree	8/10/22	8/10/22 9:50	8/12/22 7:50	-24.54	-4.65	12.66	0.020
Beulah	8/11/22	8/11/22 8:00	8/12/22 8:00	-19.50	-3.85	11.27	0.320
Engineering	8/11/22	8/10/22 9:00	8/12/22 11:00	-21.72	-3.39	5.42	0.300
Beulah	8/12/22	8/12/22 8:00	8/13/22 8:30	-7.39	-1.51	4.70	0.020
Engineering	8/12/22	8/12/22 11:00	8/13/22 9:30	-10.53	-2.12	6.42	0.020
Beulah	8/13/22	8/13/22 8:30	8/13/22 14:00	-28.92	-4.06	3.55	0.690
Engineering	8/13/22	8/13/22 9:30	8/14/22 8:30	-35.54	-5.35	7.29	0.720

Table 9.4 Late Monsoon Sample Data: 8/14/2022 – 8/21/2022

Station	Event Date	Start Date	End Date	δ^2H, ‰	$\delta^{18}O$, ‰	d-excess, ‰	Amount, in.
Beulah	8/14/22	8/13/22 14:00	8/14/22 12:30	–38.34	–7.01	17.73	0.607
Beulah	8/14/22	8/14/22 13:05	8/14/22 13:55	–39.15	–5.99	8.79	0.078
Beulah	8/14/22	8/14/22 12:30	8/14/22 13:05	–39.40	–5.05	0.96	0.112
Beulah	8/14/22	8/14/22 13:55	8/15/22 6:20	–41.98	–6.84	12.76	0.090
Engineering	8/14/22	8/14/22 8:30	8/15/22 8:30	–42.92	–7.09	13.84	1.072
Beulah	8/15/22	8/15/22 6:20	8/15/22 17:00	–26.10	–3.78	4.14	1.580
Soliere	8/15/22	8/15/22 6:45	8/16/22 6:30	–26.89	–3.96	4.79	0.350
Beulah	8/15/22	8/15/22 17:00	8/16/22 9:00	–29.95	–5.31	12.54	1.580
Engineering	8/15/22	8/15/22 8:30	8/16/22 11:45	–30.31	–4.80	8.12	0.071
Windtree	8/15/22	8/12/22 7:50	8/16/22 9:45	–43.30	–6.99	12.61	1.690
Engineering	8/17/22	8/17/22 11:45	8/18/22 11:45	–5.32	–1.42	6.06	0.103
Beulah	8/17/22	8/16/22 9:00	8/17/22 17:20	–25.56	–3.97	6.17	0.367
Windtree	8/17/22	8/16/22 9:45	8/18/22 19:00	–13.12	–2.57	7.43	
Soliere	8/18/22	8/16/22 6:30	8/19/22 7:30	–19.24	–3.46	8.43	0.070
Beulah	8/18/22	8/17/22 17:20	8/18/22 18:00	–23.04	–4.16	10.22	0.370
Engineering	8/18/22	8/18/22 11:45	8/19/22 10:30	–26.99	–4.75	11.02	0.503
Beulah	8/18/22	8/18/22 18:00	8/19/22 14:00	–47.16	–7.95	16.45	0.126
Windtree	8/19/22	8/18/22 19:00	8/19/22 15:45	–38.64	–6.43	12.80	0.280
Engineering	8/19/22	8/19/22 10:30	8/20/22 9:00	–39.39	–6.69	14.12	0.078
Soliere	8/21/22	8/21/22 7:50	8/22/22 6:30	–25.74	–3.62	3.19	0.200

Table 9.5 Late Monsoon Sample Data: 8/22/2022 – 9/13/2022

Station	Event Date	Start Date	End Date	δ^2H, ‰	$\delta^{18}O$, ‰	d-excess, ‰	Amount, in.
Beulah	8/21/22	8/19/22 14:00	8/21/22 15:00	–35.70	–6.40	15.53	0.104
Engineering	8/21/22	8/20/22 9:00	8/22/22 7:00	–41.36	–6.95	14.24	0.155
Windtree	8/21/22	8/21/22 7:50	8/22/22 12:00	–35.47	–6.68	17.95	0.140
Soliere	8/24/22	8/22/22 6:45	8/25/22 6:45	–8.71	–2.08	7.96	0.330
Windtree	8/24/22	8/22/22 12:00	8/25/22 13:00	–27.11	–4.66	10.20	0.691
Beulah	8/24/22	8/21/22 15:00	8/24/22 15:30	–33.55	–5.71	12.12	0.680
Beulah	8/25/22	8/24/22 15:30	8/25/22 13:00	–46.61	–7.70	14.99	0.225
Soliere	8/25/22	8/25/22 6:45	8/26/22 6:45	–48.58	–8.16	16.69	0.250
Windtree	8/26/22	8/25/22 13:00	8/26/22 12:00	–25.22	–5.33	17.41	0.691
Beulah	8/26/22	8/25/22 13:00	8/26/22 13:40	–35.58	–6.02	12.59	0.030
Beulah	8/27/22	8/26/22 13:40	8/28/22 9:15	–12.92	–3.05	11.48	0.079
Windtree	9/10/22	1/0/00 0:00	9/10/22 13:12	–46.02	–6.62	6.96	0.167
Beulah	9/10/22	8/28/22 9:15	9/11/22 9:00	–48.31	–5.67	-2.91	0.182
Windtree	9/10/22	9/10/22 13:12	9/11/22 7:15	–50.13	–7.41	9.18	0.395
Engineering	9/11/22	1/0/00 0:00	9/12/22 16:00	–48.19	–7.10	8.58	0.127
Windtree	9/11/22	9/11/22 7:15	9/12/22 7:15	–52.61	–5.03	-12.38	0.021
Soliere	9/12/22	9/12/22 0:00	9/13/22 10:15	–69.73	–10.39	13.42	0.182
Beulah	9/12/22	9/11/22 9:00	9/13/22 8:00	–78.01	–11.34	12.71	0.158
Beulah	9/13/22	9/13/22 8:00	9/13/22 18:00	–65.09	–9.63	11.98	0.127
Soliere	9/13/22	9/13/22 10:15	9/14/22 7:00	–70.76	–9.97	9.02	0.091

Table 9.6 Late Monsoon Sample Data: 9/13/2022 – 9/23/2022

Station	Event Date	Start Date	End Date	δ^2H, ‰	$\delta^{18}O$, ‰	d-excess, ‰	Amount, in.
Engineering	9/13/22	9/12/22 16:00	9/14/22 12:30	–74.16	–10.86	12.73	0.559
Windtree	9/13/22	9/12/22 7:15	9/14/22 12:00	–76.09	–11.11	12.80	0.359
Beulah	9/13/22	9/13/22 18:00	9/14/22 8:30	–85.22	–12.07	11.30	0.085
Beulah	9/20/22	9/13/22 8:00	9/21/22 11:30	–73.38	–10.61	11.52	0.455
Windtree	9/20/22	9/14/22 12:00	9/21/22 8:00	–76.17	–11.11	12.71	0.464
Engineering	9/20/22	9/14/22 12:30	9/22/22 8:15	–76.54	–11.16	12.76	
Soliere	9/20/22	9/14/22 7:00	9/22/22 7:45	–79.14	–11.29	11.15	
Windtree	9/21/22	9/21/22 8:00	9/22/22 8:00	–80.96	–11.19	8.55	0.262
Beulah	9/21/22	9/21/22 11:30	9/22/22 8:30	–84.02	–11.69	9.49	0.146
Soliere	9/23/22	9/22/22 7:45	9/23/22 16:45	–57.53	–7.08	-0.87	0.028

Table 9.7 Autumn Sample Data: 10/2/2022 – 11/3/2022

Station	Event Date	Start Date	End Date	δ^2H, ‰	$\delta^{18}O$, ‰	d-excess, ‰	Amount, in.
Beulah	10/2/22	9/21/22 11:30	10/3/22 10:00	-4.87	-2.47	14.88	0.913
Beulah	10/2/22	9/21/22 11:30	10/3/22 10:00	-4.87	-2.47	14.88	0.913
Engineering	10/2/22	9/22/22 8:15	10/3/22 10:15	-6.48	-3.04	17.82	0.034
Soliere	10/2/22	9/29/22 7:15	10/3/22 7:10	-20.17	-5.20	21.39	0.126
Windtree	10/3/22	10/2/22 16:00	10/4/22 11:30	-42.09	-7.01	13.97	0.691
Soliere	10/3/22	10/3/22 7:10	10/4/22 6:25	-46.94	-7.71	14.77	0.566
Engineering	10/3/22	10/3/22 10:15	10/4/22 10:40	-48.79	-8.02	15.38	0.513
Beulah	10/3/22	10/3/22 10:00	10/4/22 11:15	-48.86	-8.32	17.69	0.607
Beulah	10/6/22	10/4/22 11:15	10/7/22 10:15	-52.20	-7.76	9.91	0.117
Engineering	10/6/22	10/4/22 10:40	10/7/22 8:25	-57.09	-8.80	13.28	0.022
Soliere	10/15/22	10/13/22 8:00	10/16/22 8:45	-36.38	-6.43	15.03	0.558
Engineering	10/15/22	10/13/22 9:00	10/16/22 9:30	-42.00	-7.32	16.52	0.911
Soliere	10/16/22	10/16/22 8:45	10/17/22 9:20	-22.56	-5.25	19.43	0.042
Engineering	10/16/22	10/16/22 9:30	10/17/22 8:20	-28.23	-5.93	19.19	0.012
Soliere	10/22/22	10/17/22 9:20	10/23/22 9:15	-31.15	-5.90	16.07	0.176
Engineering	10/22/22	10/17/22 8:20	10/23/22 10:00	-36.80	-6.82	17.74	0.218
Windtree	10/22/22	10/21/22 16:00	10/23/22 8:00	-38.06	-6.55	14.38	
Soliere	11/2/22	10/23/22 9:15	11/3/22 7:30	-49.54	-8.40	17.65	0.301
Engineering	11/2/22	11/2/22 7:30	11/3/22 8:30	-48.60	-8.62	20.36	0.367
Soliere	11/3/22	11/3/22 7:30	11/4/22 6:00	-58.65	-9.55	17.76	0.033

Table 9.8 Autumn Sample Data: 11/3/2022 – 11/9/2022

Station	Event Date	Start Date	End Date	δ^2H, ‰	$\delta^{18}O$, ‰	d-excess, ‰	Amount, in.
Engineering	11/3/22	11/3/22 8:30	11/4/22 8:30	-66.42	-10.70	19.17	0.186
Windtree	11/3/22	11/3/22 7:30	11/4/22 8:00	-69.36	-10.33	13.30	0.450
Engineering	11/9/22	11/9/22 7:30	11/9/22 17:45	-48.40	-8.08	16.23	0.342
Soliere	11/9/22	11/8/22 16:30	11/10/22 7:00	-44.16	-7.35	14.63	0.228
Windtree	11/9/22	11/4/22 11:00	11/10/22 8:00	-47.37	-7.80	15.00	0.311

9.2 Appendix B: Daily Mean Values

Table 9.9 Early Monsoon Daily Data: 6/23/22 – 7/26/22

Date	No. of Obs.	d^2H (mean ± SD), ‰	$d^{18}O$ (mean ± SD), ‰	d-excess (mean ± SD), ‰
6/23/22	2	-63.84 ± 2.96	-8.19 ± 0.33	1.67 ± 0.35
6/24/22	1	-65.52	-8.36	1.34
6/26/22	2	-48.31 ± 12.81	-7.21 ± 2.49	8.19 ± 8.75
6/30/22	2	-34.64 ± 0.27	-5.23 ± 0.29	7.16 ± 2.09
7/1/22	2	-47.64 ± 10.16	-6.03 ± 2.54	0.61 ± 10.12
7/12/22	2	-18.56 ± 0.04	-2.22 ± 1.54	-0.81 ± 12.29
7/14/22	3	-7.99 ± 6.31	-1.48 ± 1.47	3.83 ± 5.76
7/15/22	1	-1.56	-0.28	0.64
7/16/22	3	-9.99 ± 8.19	-1.48± 1.39	1.81 ± 7.52
7/17/22	1	-37.22	-6.23	12.60
7/19/22	1	5.85	0.75	-0.17
7/21/22	2	-4.30 ± 4.87	0.06 ± 0.33	-4.78 ± 7.48
7/22/22	2	0.33 ± 19.80	-0.24 ± 3.15	2.29 ± 5.39
7/23/22	2	9.34 ± 0.98	0.95 ± 0.38	1.72 ± 4.00
7/24/22	3	-22.91 ± 9.09	-5.03 ± 1.27	17.34 ± 7.01
7/25/22	2	-12.10 ± 1.81	-2.87 ± 0.64	10.83 ± 6.92
7/26/22	1	-17.65	-3.88	13.42

Table 9.10 Early Monsoon Daily Data: 7/27/22 – 8/13/22

Date	No. of Obs.	d^2H (mean ± SD), ‰	$d^{18}O$ (mean ± SD), ‰	d-excess (mean ± SD), ‰
7/27/22	2	-7.70 ± 5.13	-2.17 ± 0.92	9.68 ± 2.27
7/28/22	3	-21.35 ± 3.30	-3.88 ± 0.55	9.73 ± 1.37
7/29/22	5	-34.18 ± 3.32	-5.84 ± 0.50	12.54 ± 1.40
7/30/22	2	-41.43 ± 11.54	-6.93 ± 1.33	13.98 ± 0.91
8/7/22	1	-6.95	0.35	-9.76
8/8/22	1	-3.21	-0.38	-0.20
8/9/22	2	-14.35 ± 6.01	-2.73 ± 1.14	7.50 ± 3.09
8/10/22	3	-19.99 ± 5.57	-3.45 ± 1.16	7.63 ± 4.37
8/11/22	2	-21.92 ± 2.53	-3.96 ± 0.64	8.35 ± 4.14
8/12/22	2	-8.96 ± 2.22	-1.82 ± 0.43	5.56 ± 1.22
8/13/22	2	-32.23 ± 4.68	-4.71 ± 0.92	5.42 ± 2.64

Table 9.11 Late Monsoon Daily Data

Date	No. of Obs.	d^2H (mean ± SD), ‰	$d^{18}O$ (mean ± SD), ‰	d-excess (mean ± SD), ‰
8/14/22	5	-40.36 ± 1.98	-6.40 ± 0.87	10.81 ± 2.75
8/15/22	5	-31.31 ± 6.95	-4.97 ± 1.29	8.44 ± 3.88
8/17/22	3	-14.67 ± 10.21	-2.65 ± 1.27	6.55 ± 0.08
8/18/22	3	-20.60 ± 5.90	-4.12 ± 0.65	9.32 ± 1.41
8/19/22	3	-41.73 ± 4.71	-7.02 ± 0.81	14.46 ± 1.85
8/21/22	4	-34.57 ± 6.49	-5.91 ± 1.55	12.73 ± 6.54
8/24/22	3	-23.13 ± 12.89	-4.15 ± 1.87	10.09 ± 2.08
8/25/22	2	-40.14 ± 12.95	-7.93 ± 0.32	15.84 ± 1.20
8/26/22	2	-30.40 ± 7.32	-5.67 ± 0.49	15.00 ± 3.41
8/27/22	1	-12.92	-3.05	11.48
9/10/22	3	-48.15 ± 2.06	-6.57 ± 0.87	4.41 ± 6.98
9/11/22	2	-50.40 ± 3.13	-6.06 ± 1.46	-1.90 ± 14.82
9/12/22	2	-73.87 ± 5.86	-10.87 ± 0.67	13.07 ± 0.50
9/13/22	5	-74.26 ± 7.41	-10.73 ± 0.96	11.57 ± 1.78
9/20/22	4	-76.31 ± 2.36	-11.04 ± 0.30	12.04 ± 0.82
9/21/22	2	-82.49 ± 2.16	-11.44 ± 0.35	9.02 ± 5.23
9/23/22	1	-57.53	-7.08	-0.87

Table 9.12 Autumn Daily Data

Date	No. of Obs.	d^2H (mean ± SD), ‰	$d^{18}O$ (mean ± SD), ‰	d-excess (mean ± SD), ‰
10/2/22	3	-10.51 ± 8.41	-3.57 ± 1.44	18.03 ± 3.26
10/3/22	4	-46.67 ± 3.18	-7.77 ± 0.56	15.45 ± 1.60
10/6/22	2	-54.64 ± 3.45	-8.28 ± 0.73	11.60 ± 2.38
10/15/22	2	-39.19 ± 3.97	-6.87 ± 0.63	15.77 ± 1.06
10/16/22	2	-25.39 ± 4.01	-5.59 ± 0.48	19.31 ± 0.17
10/22/22	3	-35.34 ± 3.68	-6.42 ± 0.47	16.06 ± 1.68
11/2/22	2	-49.07 ± 0.66	-8.51 ± 0.16	19.00 ± 1.92
11/3/22	3	-64.81 ± 5.53	-10.19 ± 0.59	16.74 ± 3.07
11/9/22	3	-46.64 ± 2.21	-7.74 ± 0.37	15.29 ± 0.84